Fiducial Reference Measurements for Ground-Based DOAS Air-Quality Observations

ESA Contract No. 4000135355/21/I-DT-lr

Deliverable D3.2:

Technical Note (TN) on the validation of FRM4DOAS aerosol retrieval products

Date: 28/07/2025

Version: 1.1

Contributing authors:

U. Frieß (IUP-HD)

T. Wagner, S. Ziegler and S. Beirle (MPIC)

M. Friedrich, and M. Van Roozendael (IASB-BIRA)

A. Piters (KNMI)

A. Bais and D. Karagkiozidis (AUTH)

Content

2 Acronyms and abbreviations

Acronyms and abbreviated terms that are specific for this document can be found below.

AOD	Aerosol optical depth
APS	Aerodynamical Particle Sizer
Aeronet	Aerosol Robotic Network
CINDI	Cabauw Intercomparison of UV-Vis DOAS Instruments
DOAS	Differential Optical Absorption Spectroscopy
dSCD	Differential Slant Column Density
ICAD	Iterative Cavity-Enhanced DOAS
MAPA	Mainz Profile Algorithm
MAX-DOAS	Multi-Axis Differential Optical Absorption Spectroscopy
MAAP	Multi-Angle Absorption Photometer
MMF	Mexican MAX-DOAS Fit
OEM	Optimal estimation
RAPSODI	Retrieval of Atmospheric Parameters from Spectroscopic Observations using Doas Instruments
SMPS	Scanning Mobility Particle Sizer
TIP	Technical implementation plan
VMR	Volume mixing ratio

1 Introduction

The objective of FRM$_4$DOAS WP3 is the development of a consolidated MAX-DOAS aerosol product and the documentation of the essential steps for the optimisation as a TIP. The FRM$_4$DOAS data product includes two distinctively different aerosol vertical profile products, namely the OEM-based MMF algorithm (Friedrich et al., 2019) and the parametrised MAPA algorithm (Beirle et al., 2019). This document describes the validation of these data product in terms of direct inter-comparison of MAPA and MMF data products as well as validation of both products with independent aerosol-related observations at the different measurement sites. As a first step of WP3, an Ancillary Data Availability Survey has been performed among the FRM$_4$DOAS participants. The results of this assessment can be found in the corresponding deliverable D3.1. The results of this survey with the available ancillary data at the different sites are summarised in Table 1.

	Sun Photometer	Ceilometer	Lidar	SMPS/APS	Nephelometer	Transmissometer	MAAP	Particulate Matter	Meteorology	Ballon Soundings	Remarks
Cabauw	■	■	■	■	■	■	■	■	■	■	Raman Lidar@355, 387, 407, 530, 532, 607, 1064 nm - 500 m overlap
Uccle	■	■	■		■		■	■	■	■	
Lauder	■	■	■	■					■	■	Not part of FRM4DOAS consortium
Mainz	■	■							■		
Thessaloniki	■		■					■			Raman Lidar @ 355, 387, 532, 607, 1064 nm - 800 m overlap
Neumayer		■							■	■	
Xianghe	■										
Bremen											
Ny-Alesund											
Arrival Heights											

Validation sites

Table 1: Aerosol-related ancillary measurements at the FRM4DOAS sites. The red frame indicates the sites selected for primary validation. Adapted from the Ancillary Data Availability Survey Report (D3.1).

Cabauw, Uccle, Lauder, Mainz and Thessaloniki were identified as suitable validation sites and ancillary data was collected from these sites. The validation activities focused on a comparison of FRM$_4$DOAS AOD and aerosol extinction profiles with co-located sun photometer and Lidar/Ceilometer measurements, respectively. Furthermore, a direct comparison between MAPA and MMF products was performed for all available stations within the FRM$_4$DOAS network.

The MAPA data product as part of the FRM$_4$DOAS product files consists of different sub-products: MAPA_SF_0.8 applies a fixed O_4 scaling factor of 0.8, MAPA_SF_1.0 applies an O_4 scaling factor of 1.0 (i.e., the O_4 dSCDs are kept unscaled), and O4_VAR applies a variable scaling factor that is retrieved by the MAPA algorithm during the optimisation process. All three MAPA data products are included in the validation and intercomparison.

.

This document is structured as follows: The availability of FRM$_4$DOAS aerosol data products and ancillary data will be summarised in Section 2. The performance of the FRM$_4$DOAS aerosol flagging scheme is investigated in Section 3. The inter-comparison and validation of MAPA and MMF AODs is presented in Section 4, and a comparison of the aerosol extinction profiles with co-located Ceilometer measurements is presented in Section 5. Investigations on the choice of the optimal viewing geometry and the vertical retrieval grid are presented in Section 0.

2 Data availability

The intercomparison and validation presented here is based on FRM_4DOAS level 1 product files from all available stations for the period between June 2018 and August 2022. Aeronet AOD data and Ceilometer backscatter profiles were collected whenever available. The availability of FRM_4DOAS data products and ancillary measurements for the 360 nm and 477 nm aerosol data products are shown in Figures 1 and 2, respectively. In total, the inter-

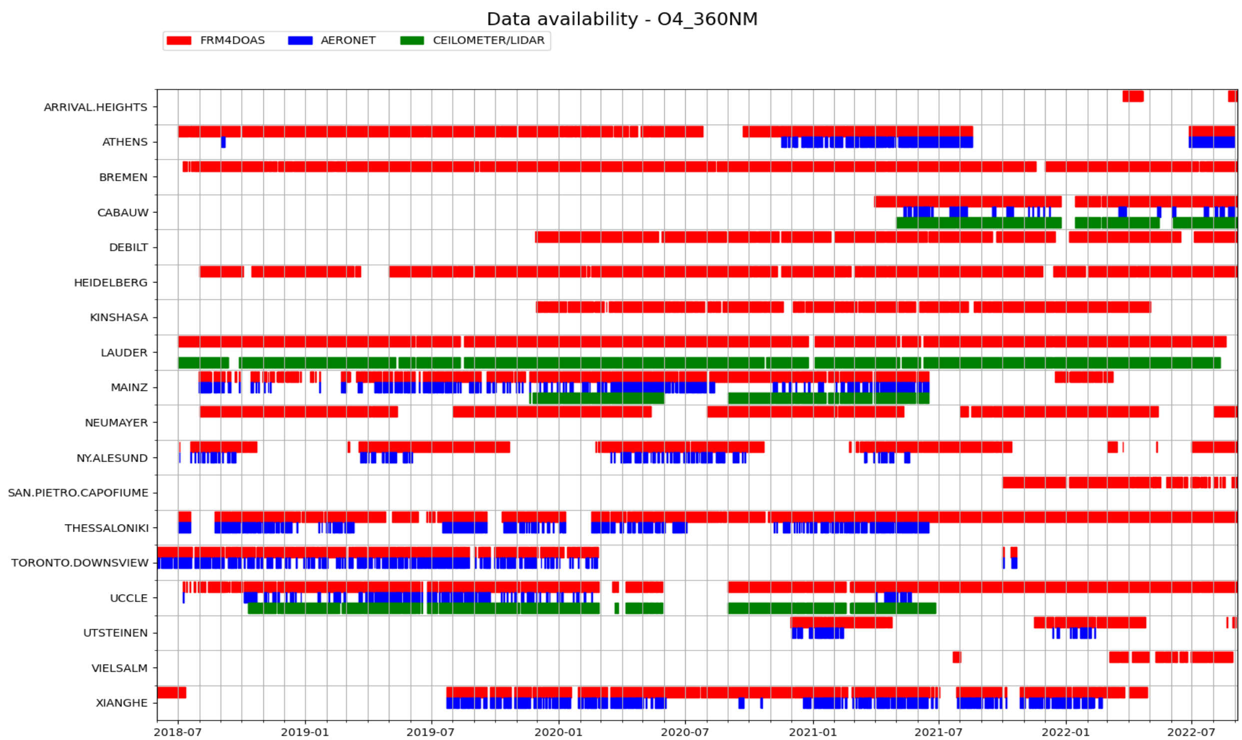

Figure 1:Data availability for the UV (360 nm) aerosol data product. Red: FRM_4DOAS 360 nm aerosol extinction profiles; Blue: Aeronet AOD; green: Ceilometer backscatter vertical profiles.

comparison and validation encompasses about 2.5 million aerosol extinction profiles. The number of profiles from each station, together with the number of ancillary data, are listed in Table 2.

In addition to the data listed here, a Raman lidar is available for the Thessaloniki site. Data from this instrument has, however, not been included in the intercomparison because of the large overlap region up to an altitude of more than 800 m, where this LIDAR instrument has no sensitivity.

Figure 2: Same as Figure 1, but for aerosol products at 477 nm.

3 Assessment of the FRM4DOAS flagging scheme

In order to provide a measure for the quality of the FRM_4DOAS data products, a number of different flags are available in the L1 product files. Apart from detailed flags, which are different for MAPA and MMF, overall quality flags are available for both algorithms. These can assume values between 0 and 2, with 0 representing valid data, 1 representing a warning, and 2 erroneous data.

The MAPA flagging scheme is based on various sub-flags, checking for criteria such as missing data, agreement between measurement and forward model, consistency of the distribution of derived profile parameters, and profile shape. The total flag merges these different warnings or errors. Details about the MAPA flagging scheme can be found in Beirle et al., 2019.

In addition to the flags provided by MAPA and MMF, the FRM_4DOAS L1 data product also contains a broken cloud flag, with 40% of the data being flagged as being affected by broken clouds. The broken cloud flag has, however, only little impact on the distribution of the validity flag (see Figure 1) and the overall data quality.

The distribution of quality flags for MAPA and MMF are distinctively different. Virtually no MMF data (< 0.1%) are flagged as valid, while this is the case for 17% – 30% of MAPA data (depending on algorithm and wavelength). This indicates that the MMF flagging scheme is too strict and that a revision of the flagging algorithm is required in order to provide a certain number of profiles that can be considered as useful for the end user.

Given the very low number MMF data points with a valid QA flag, it has been decided to consider MMF data as valid if the overall quality flag value is either “valid” or “warning”, resulting in 35% and 43% of valid data for UV and Vis, respectively. For MAPA, which has a reasonable number of valid data points, only data flagged as valid are considered.

In order to consider the same subset of measurements for both algorithms, the validation and intercomparison data set is further restricted to instances where MAPA and MMF data are both valid according to the aforementioned selection criteria. This leaves only 4.5% (UV) and 8.6% (Vis) of the total amount of data for the intercomparison. This small overlap indicates that MAPA and MMF flagging schemes are sensitive to different factors.

The histograms of the AOD error for the different FRM$_4$DOAS retrieval algorithms shown in Figure 2 show only little dependency of the quality flag for MMF (“warning” or “error”), whereas the quality criteria for MAPA are strongly dependent on the AOD error, with AOD errors for data flagged as valid being smaller than 0.2.

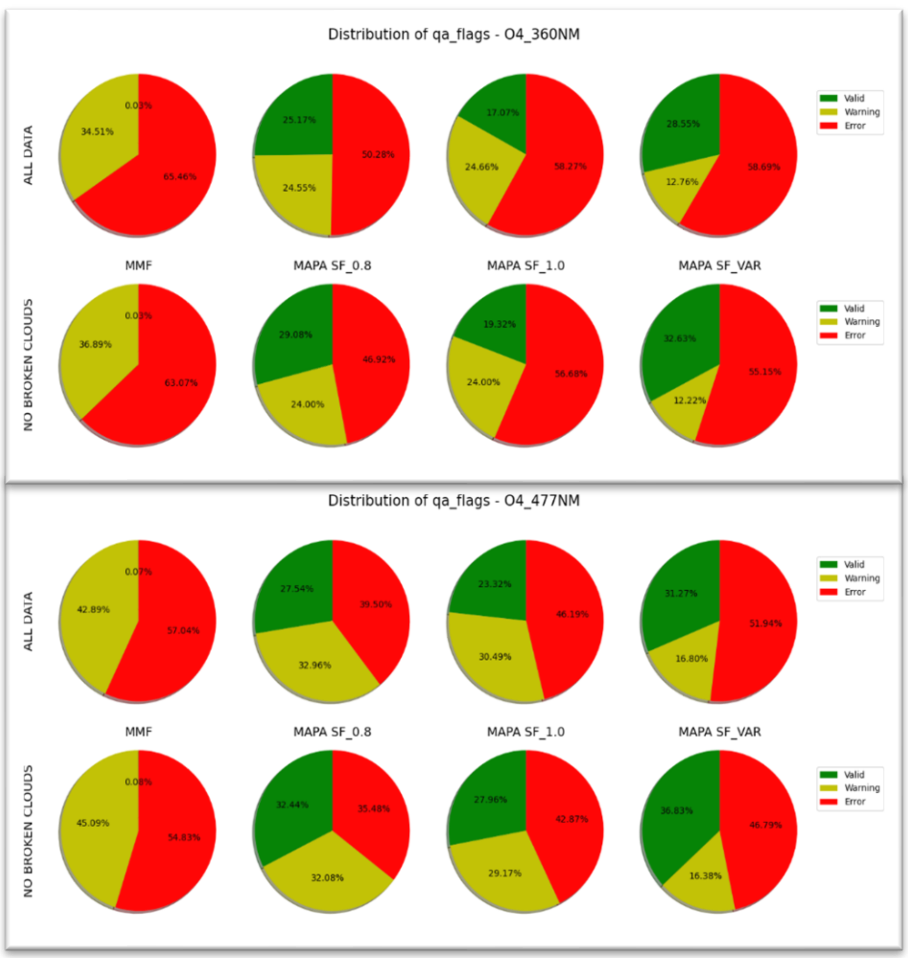

Figure 1: Distribution of the quality flag values for MMF and the tree MAPA aerosol data products at 360 nm (top) and 477 nm (bottom). Pie charts are shown for all data (top rows) and data flagged as not affected by broken clouds (bottom rows).

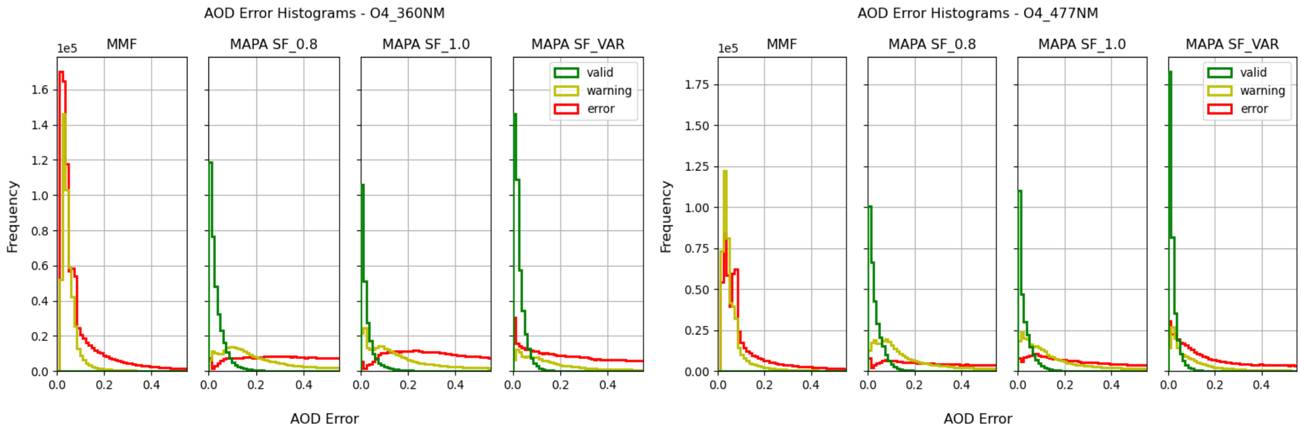

Figure 2: Histograms of the AOD error for the different overall quality flag values for MMF and the three versions of MAPA. Left: UV; right: Vis.

4 Validation of the Aerosol Optical Depth

4.1 AOD intercomparison between MAPA and MMF

In this section, a direct comparison of the AOD values from MMF and MAPA is presented. It needs to be noted that both algorithms determine the AOD differently: MMF retrieves aerosol extinction profiles from the surface up to 4 km in layers of 200 m thickness based on an OEM algorithm and reports the integrated profile, whereas MAPA retrieves a set of parameters for the shape of the profile, which is of exponential shape at the top, and reports the AOD based on these parameters (see Beirle et al., 2019). Thus, MAPA AOD also includes information on aerosols above 4 km altitude, while this altitude region is not part of the MMF state vector.

Figure 3 shows correlation plots between the AOD from MMF and the three versions of the MAPA algorithms for all stations using only quality filtered data. Slope and intercept were determine using orthogonal distance regression (ODR) since both data sets can be considered as independent. Correlation plots for each individual station can be found in Appendix 9.1. Correlation coefficients range between R = 0.66 (MMF versus MAPA SF_1.0 in the visible) and R = 0.83 (MMF versus MAPA SF_0.8 in the UV). The AOD from MAPA is significantly larger than from MMF, with slopes of the linear regression ranging between 1.33 (MMF versus MAPA SF_VAR in the visible) and 2.34 (MMF versus MAPA SF_1.0 in the UV). This discrepancy is higher in the UV, where the MAPA AOD is about twice the MMF AOD, which is far beyond what can be expected from the uncertainties of the retrieval algorithms or systematic impacts, such as the missing sensitivity of MMF to altitudes above 4 km.

Despite the fact that MMF applies no scaling factor, the correlation between MAPA and MMF is significantly better if a variable scaling factor or a scaling factor of 0.8 is applied by MAPA algorithm.. The slope is generally closer to unity in the Vis than in the UV.

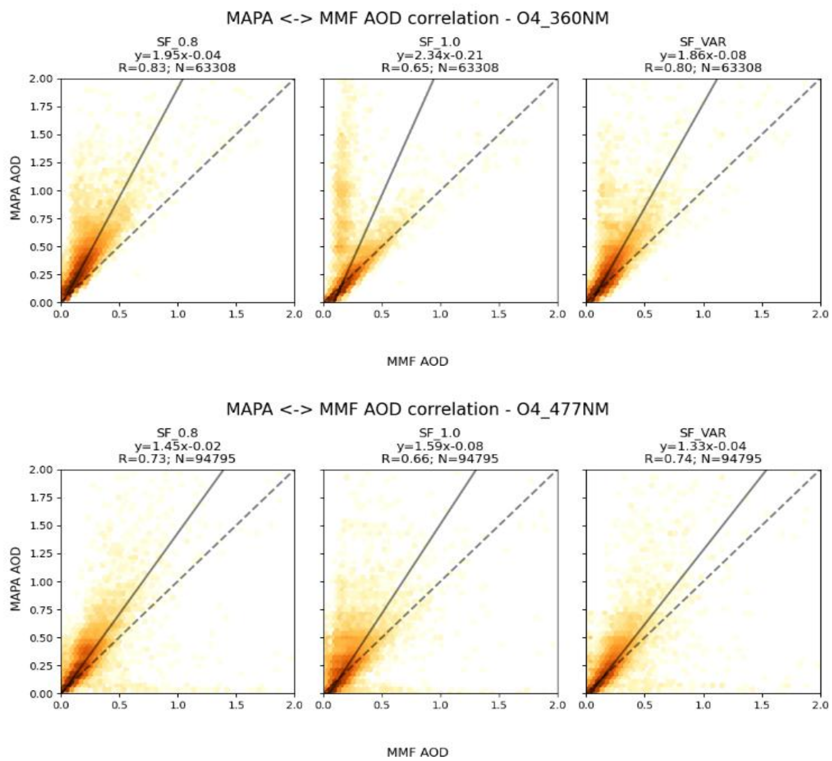

Figure 3: Comparison of AOD from MMF (x-axis) with the AOD from the three versions of MAPA (y-axis) in the UV (top) and Vis (bottom) for valid data only. The colours (from light red to dark red) indicate the density of data points Slope, intercept, regression coefficient and number of data points are shown at the top of each panel.

The parameters of an orthogonal distance regression between MAPA and MMF AOD for each station are shown in Figure 4. The level of agreement differs significantly between the different stations, but is in general better for individual stations than for the entire data from all station discussed above, with regression coefficients and slopes close to unity for various station. This is partly due to the fact that the Athens instrument with most data points, which therefore dominates the statistics, shows relatively poor agreement between MAPA and MMF. The regression coefficients are usually closer to unity in the UV than in the visible, which might be due to the fact that measurements in the visible are more sensitive to horizontal inhomogeneities due to the longer light paths.

In the UV, some stations yield regression parameters and slopes very close to unity. This includes Lauder, Ny Alesund, and Uccle. There is no clear relationship between the level of agreement between MAPA and MMF to the level of pollution and/or rural and urban sites. Parts of these discrepancies are possibly caused by the quality of the spectral data. MAPA SF0.8 and SF_VAR products generally yield better agreement to MMF than the MAPA SF1.0 product. This may indicate that a scaling of the O_4 cross section is necessary, but it is unclear why this yields a better agreement to MMF, which uses an unscaled O_4 cross section.

	UV				VIS			
Site	FRM4DOAS	AERONET	CEILO	CEILO+AERONET	FRM4DOAS	AERONET	CEILO	CEILO+AERONET
ARRIVAL.HEIGHTS	332	0	0	0	305	0	0	0
ATHENS	342073	66840	0	0	341816	67284	0	0
BREMEN	72432	0	0	0	72345	0	0	0
CABAUW	69378	9630	61984	9185	18932	2437	17556	2338
DEBILT	60060	0	0	0	72419	0	0	0
HEIDELBERG	52380	0	0	0	52337	0	0	0
IZANA	0	0	0	0	43489	31303	0	0
KINSHASA	44590	0	0	0	45046	0	0	0
LAUDER	103652	0	0	0	102357	0	0	0
MAINZ	184377	59825	87430	27745	0	0	0	0
NEUMAYER	34608	0	0	0	34198	0	0	0
NY.ALESUND	71599	5629	0	0	71152	5514	0	0
SAN.PIETRO.CAPOFIUME	51021	0	0	0	56081	0	0	0
THESSALONIKI	121876	34659	0	0	36007	3895	0	0
TORONTO.DOWNSVIEW	57609	9768	0	0	57542	9233	0	0
UCCLE	76147	3796	33886	78	47244	3812	26105	78
UTSTEINEN	23471	2090	0	0	23298	2170	0	0
VIELSALM	11588	0	0	0	0	0	0	0
XIANGHE	25366	8206	0	0	29230	8381	0	0
TOTAL	1402559	200443	183300	37008	1103798	134029	43661	2416

Table 2: Number of available FRM$_4$DOAS profiles as well as Ceilometer and Aeronet data.

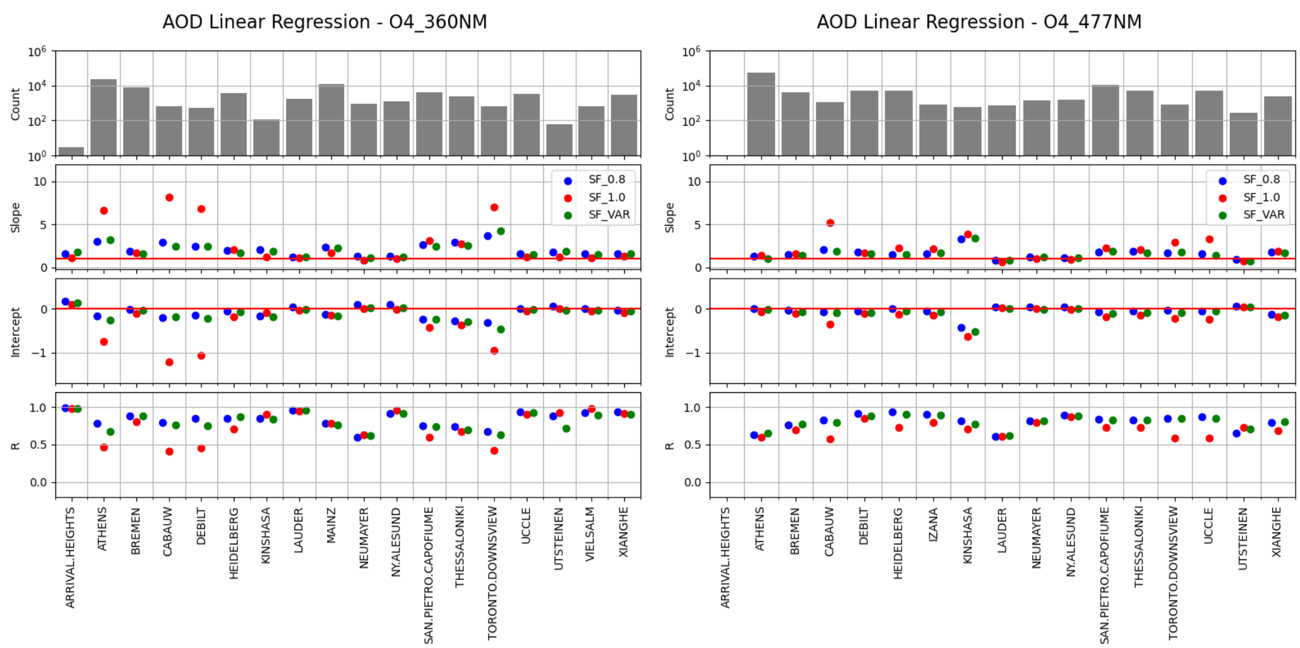

Figure 4: Linear regression parameters for the correlation between MAPA and MMF AOD for each station. Left: UV; right: Vis. The panels show (from top to bottom) the number of data points, slope, intercept and regression coefficient. Horizontal red lines show the optimal values (unity slope and zero intercept).

4.2 Consistency of reported AOD values

Figure 5 shows the correlation between the AOD values reported in the FRM$_4$DOAS L1 product files and the integrated extinction profiles for all valid data. MMF AODs and integrated profiles are consistent[1], whereas the integrated MAPA profiles are systematically smaller than the reported AOD. This is to be expected because the MAPA AOD is derived from the parametrised retrieval, allowing for aerosols to be present also above the retrieval domain (0 – 4 km).

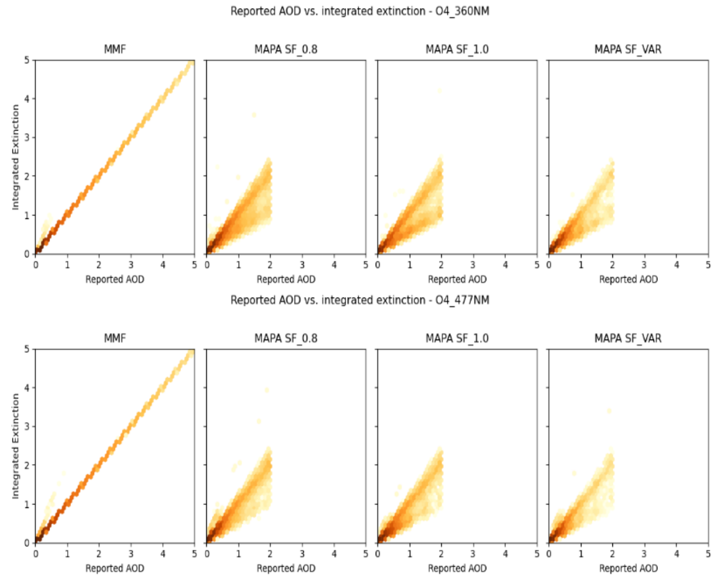

Figure 5: Correlation between reported AOD (x-axis) and AOD from integrated aerosol extinction profiles (y-axis).

However, the current output of MAPA results within FRM4DOAS has been found to be inconsistent, as the "best" (of all matching parameter combinations) AOD is provided, but the "weighted mean" (of all matching parameter combinations) profile. This inconsistency has been fixed by a revised configuration file for the MAPA output, providing "best" and "weighted_mean" for both AOD and profiles in order to allow for consistent comparisons between AOD and integrated profiles. This revised configuration will be invoked operationally within the next update of the FRM4DOAS processor.

MAPA AODs are restricted to values below 2 since this is one of the criteria of the MAPA quality flag.

[1] Note that A small percentage of days from certain instruments were delivered twice due to the submission of two different Level 1 versions, which differed slightly in their start and/or stop times. As a result, two distinct files were generated for the same period. Because the datetime stamps were identical for some scans, this led to a duplication of data, with each height bin being counted twice for those specific scans. Consequently, a small proportion of scans integrate to exactly twice the correct value. This duplication accounts for the data points in Figure 7 for MMF that deviate from the 1:1 line.

4.3 Validation with AOD from co-located sun photometer instruments

Co-located sun photometer observations are available for 10 sites (see Table 2), of which all except the instrument located at Lauder/New Zealand are part of the Aeronet network. The correlation between FRM4DOAS and sun photometer AOD at Lauder turned out to be very poor (see Figure 7). Therefore, Lauder has been excluded from the intercomparisons presented in this section. The comparison with Aeronet has been performed by selecting the Aeronet measurements closest in time to the MAX-DOAS measurement, but not more than 15 minutes apart. The Aeronet AOD has been converted to the wavelengths of the FRM_4DOAS aerosol data products (360 nm and 477 nm) using the Angström coefficient which is part of the Aeronet data products.

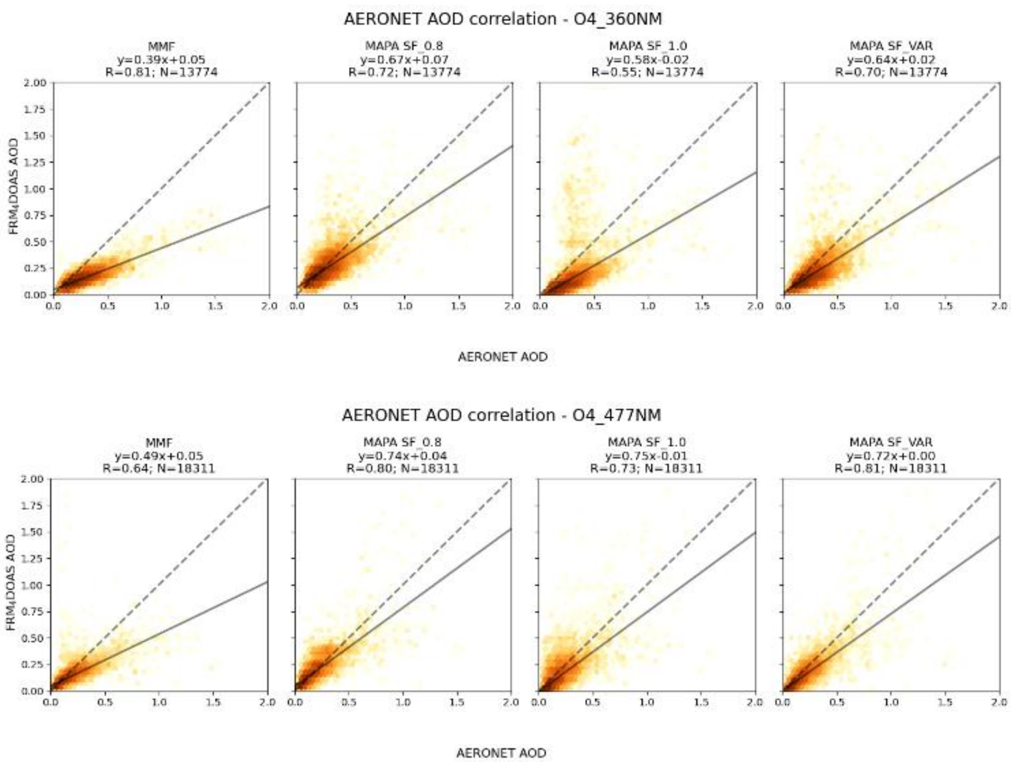

Figure 6: Comparison of AOD from Aeronet (x-axis) with the FRM_4DOAS AOD data products (y-axis) in the UV (top) and Vis (bottom). Top panels show all data, centre panels valid data only, and bottom panels valid data flagged as not contaminated by broken clouds. The colours (from light red to dark red) indicate the density of data points. Slope, intercept, regression coefficient and number of data points are shown at the top of each panel.

The correlation between Aeronet and FRM_4DOAS AOD for all stations is shown in Figure 6. Correlation plots for each individual station can be found in Appendix 9.2. The regression lines were determined using simple linear regression since one can consider the Aeronet AOD as the true value.

The AOD is significantly underestimated by the MMF algorithm, with slopes of the regression lines between MMF and Aeronet amounting to only 0.39 and 0.49 in the UV and Vis, respectively. The MMF regression coefficient in the UV (R = 0.81) is, however, significantly closer to unity than those of the tree MAPA data products (R <= 0.72), while it is poorer in the visible (MMF: R = 0.64, MAPA: R >= 0.72), indicating that the underestimation of the AOD by MMF is the result of a systematic error.

Best agreement between MAPA and Aeronet AOD is achieved for MAPA SF_0.8 and MAPA SF_VAR. Furthermore, in the slope of the regression line in the visible is smaller for SF_1.0 (0.58) than for SF_0.8 (0.72) and SF_VAR

(0.70). These findings provide further indication that an O_4 scaling factor is necessary for a realistic retrieval of the AOD.

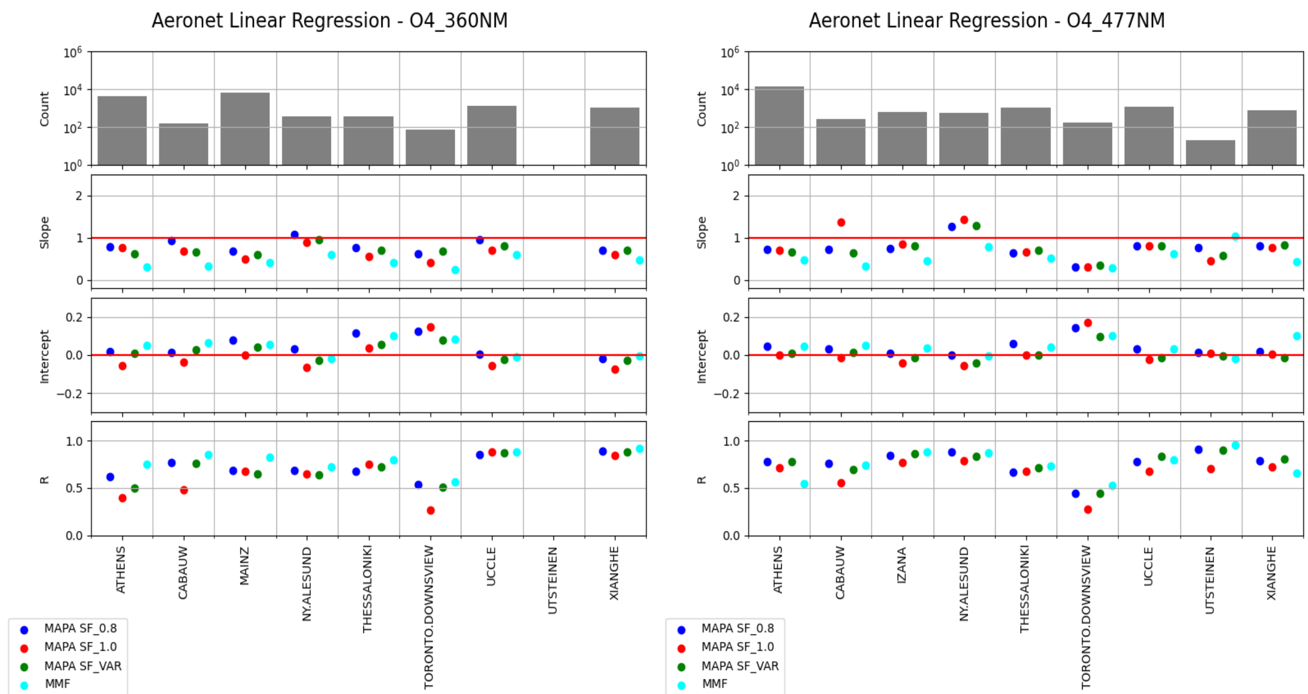

Figure 7: Linear regression parameters for the correlation between FRM$_4$DOAS and sun photometer AOD for each site.

The regression parameters for each site where co-located sun photometer measurements are available are presented in Figure 7. The level of agreement varies from site to site, with better agreement in the visible than in the UV. The AOD is systematically underestimated by the MMF algorithm at all stations (slope < 1), while the regression coefficient is equally good or even slightly better than for the MAPA data products except for Athens and Xianghe in the visible, which are both strongly polluted sites. Particularly good agreement both for MMF, MAPA SF_0.8 and MAPA SF_VAR in terms of slope, intercept and regression coefficient is found for the stations Uccle and Xiange in the UV, as well as Izana, Ny Alesund, and Utsteinen in the visible.

5 Validation of the aerosol extinction profiles

5.1 Comparison of MAPA and MMF aerosol extinction vertical profiles

Box-whisker plots of the difference in retrieved extinction between MAPA and MMF in each retrieval layer are shown in Figure 8 and, for the sake of better readability of the data, in Figure 9 with a symlog axis scale. Reasonable agreement is achieved between MMF and MAPA SF_1.0, which is to be expected since both data sets are retrieved without scaling of the O_4 cross section. In contrast, extinction values retrieved by MAPA SF_0.8 and MAPA SF_VAR are significantly higher than those from MMF, in particular in the lowermost 2 km. The discrepancy is higher in the UV than in the visible, where a maximum difference between MAPA SF_0.8/SF_VAR and MMF occurs in the 300 m layer with a median value of 0.08 km^{-1}. There are several cases where MMF shows significantly higher values than MAPA in the uppermost retrieval layers, which turn out to be caused by an instability of the MMF algorithm, see Section 5.2.

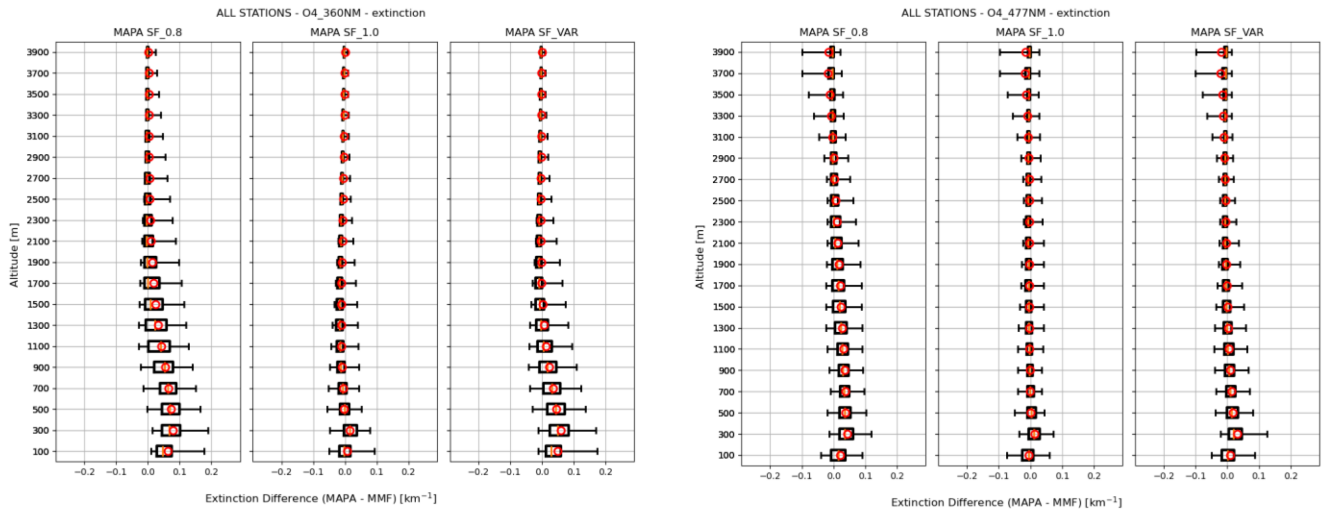

Figure 8: Box-whisker-plot of the difference between MAPA and MMF extinction for each altitude layer at 360 nm (left) and 477 (right) for all available FRM$_4$DOAS stations. Boxes and whiskers show the (25 - 75)th and (5 – 95)th percentile, respectively, in each retrieval layer. Median and mean of the data are shown as orange vertical bars and red open circles, respectively. Only profiles where both MMF and MAPA flags are valid are considered.

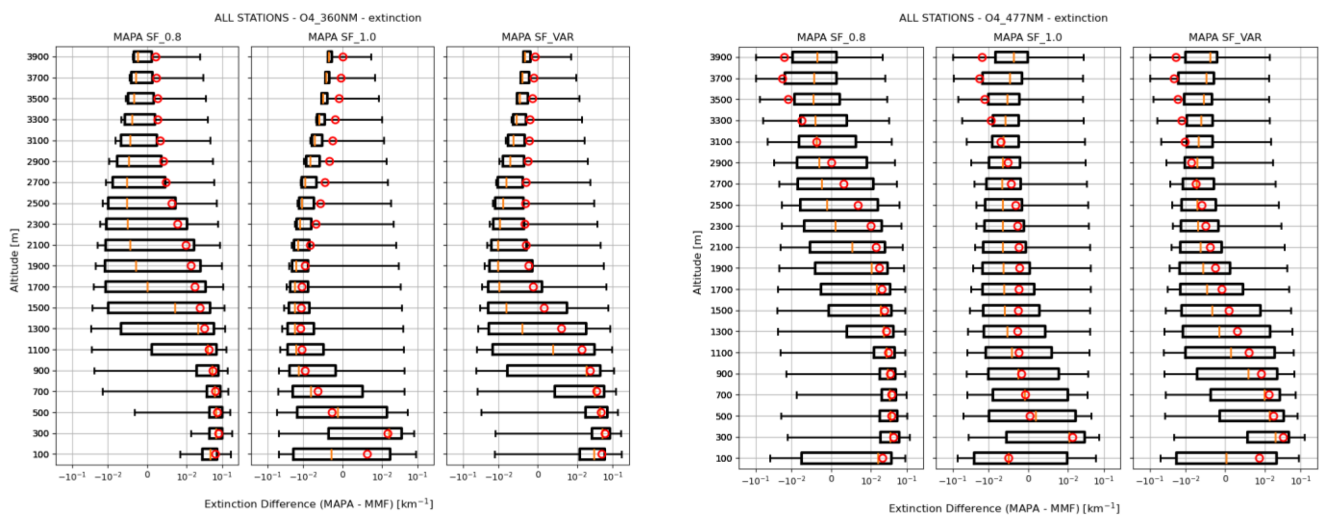

Figure 9: Same as Figure 8, but x-Axis in symlog scale, with a linear scale for -0.01 km^{-1} < x < 0.01 km^{-1}, and a logarithmic scale for |x| > 0.01 km^{-1}. Note that, in contrast to Figure 8, the apparent size of the boxes and whiskers does not correspond to the number of datapoints in each of the percentile intervals.

5.2 Validation of aerosol extinction vertical profiles with co-located Ceilometer data

Co-located measurements of backscatter profiles for the comparison with FRM$_4$DOAS aerosol extinction profiles are available for the Cabauw, Mainz and Uccle stations. The following steps were performed in the processing of the backscatter profiles prior to the validation:

1. Range-corrected backscatter profiles from co-located Ceilometer instruments closest in time to the MAX-DOAS profiles were chosen, with a maximum time distance of 10 minutes.
2. This yields > 180,000 coincident Ceilometer/FRM_4DOAS aerosol profiles in the UV > 40,000 profiles in the visible (see Table 2).
3. These profiles were binned to the FRM_4DOAS vertical grid by averaging the backscatter signal in each height level of 200 m thickness.
4. To allow for a quantitative comparison between ceilometer and MAX-DOAS profiles, the binned backscatter profiles were scaled with the AOD of co-located sun photometer instruments. Since this step requires coincident measurements by Aeronet Ceilometer, only 37,008 and 2,416 profiles in the UV and Vis, respectively, remain available for a direct comparison (see Table 2). This data product is in the following referred to as *scaled ceilometer profile*.
   Note that it was not possible to apply a partial AOD correction, as proposed by Tirpitz et al. [2021], owing to the high level of noise of many backscatter profiles at higher altitudes, in particular during cloudy conditions.
5. In order to account for the limited vertical resolution of MAX-DOAS aerosol profiles, and in particular the low sensitivity for higher altitudes, the scaled ceilometer profiles were convoluted with the MMF averaging kernels following the recommendations of Rodgers and Connor [2003]:
   $$x' = x_a + \boldsymbol{A}(x - x_a)$$
   with x_a being the MMF a priori aerosol extinction profile, $\boldsymbol{A}$ the MMF averaging kernel matrix, and x the scaled ceilometer profile. The *convoluted ceilometer profile* x' represents the vertical profile that would have been retrieved if the true profile was x. This is the mathematically correct way to compare ceilometer and MMF profiles under the assumption that the vertical resolution of the Ceilometer profiles is much higher than the one from MMF. MAPA, however, uses a parametrised approach without a priori, which is likely to have a sensitivity that is different from MMF but that also shows a decrease with altitude.

The level of agreement between the FRM_4DOAS extinction profiles and the convoluted ceilometer profiles provides a measure for the accuracy of the retrieval, whereas a comparison to the scaled ceilometer profile represents a comparison with what can be considered as the true extinction profile.
Figure 10 shows a time sample series of aerosol profiles from Ceilometer, MMF and MAPA during June 2021 in Cabauw. The MMF algorithm is able to reproduce the vertical structure of the boundary layer even under less favourable conditions. For example, on 5. June a layer of strongly enhanced backscatter near the surface, probably caused by clouds or high fog, is detected by MMF as enhanced extinction in the same altitude region, although the MMF profiles are flagged as erroneous during this day. At the same time, MAPA profiles indicate the complete absence of aerosols while the profiles are also flagged as erroneous. In contrast to MAPA, MMF is also able to correctly reproduce uplifted aerosol layers and/or clouds such as on 11. June and the morning of 12. June.

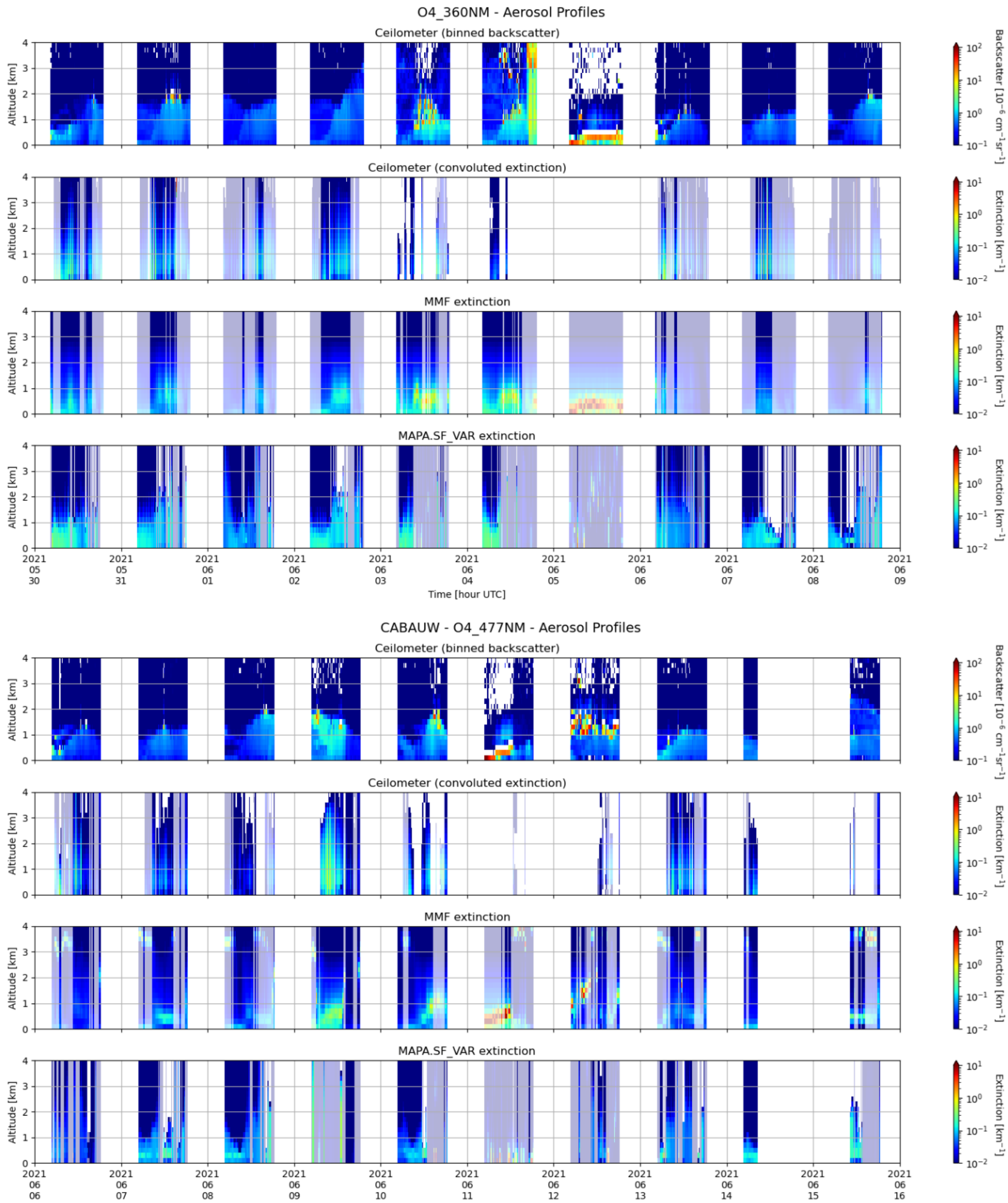

Figure 10: Example time series of Ceilometer and FRM$_4$DOAS aerosol extinction profiles for Cabauw in the UV (top) and Vis (bottom) for two different periods in June 2021. The panels show from top to bottom: (1) Ceilometer profiles binned on 200 m altitude grid; (2) Convoluted ceilometer profiles; (3) MMF profiles; (4) MAPA profiles. Profiles flagged as invalid are shown in pale colours. The MMF quality flag applies to the convoluted ceilometer profiles as well. Convoluted Ceilometer profiles are only available if sun coincident photometer AOD measurements were performed.

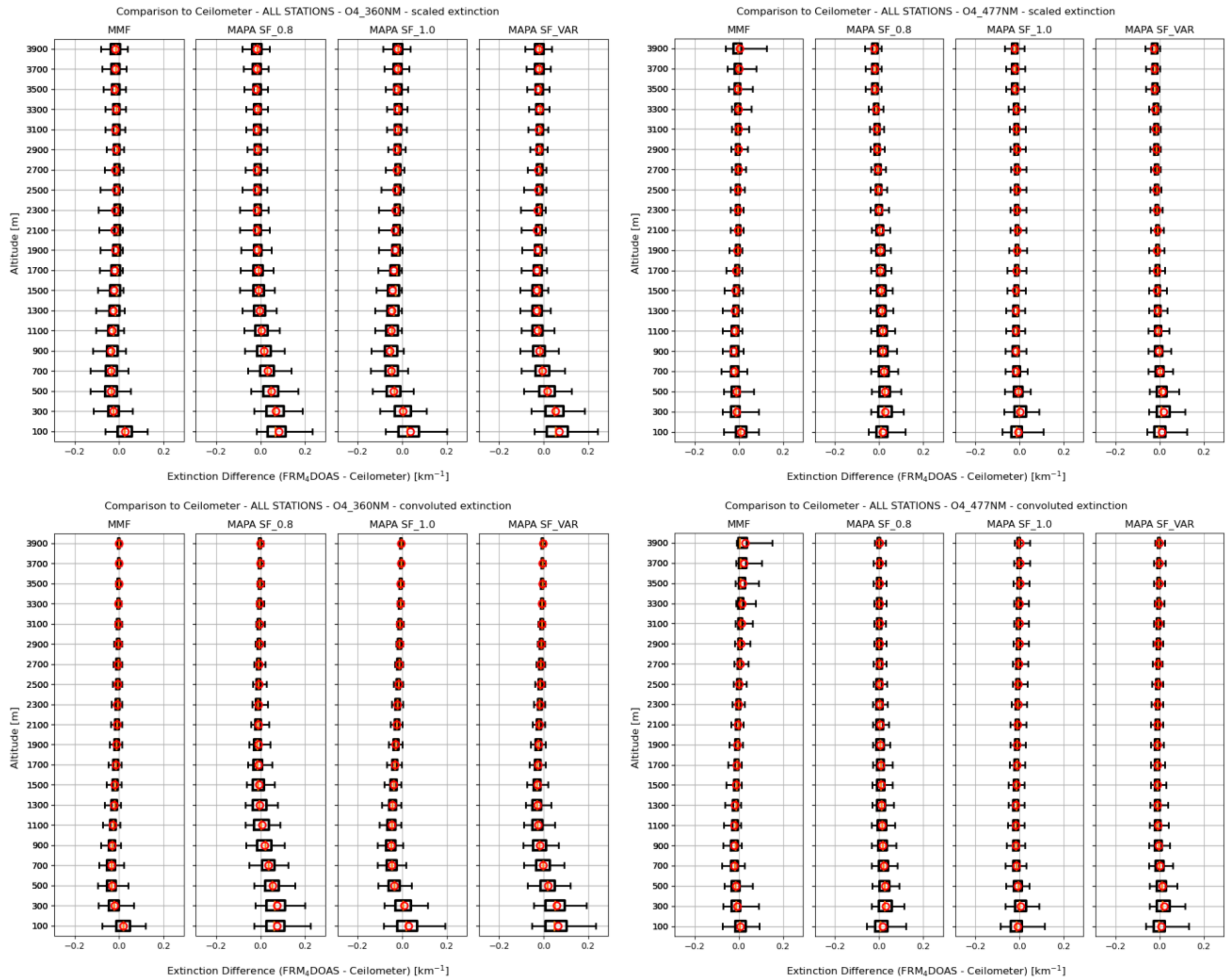

Figure 11: Box-whisker plots of differences between FRM$_4$DOAS and Ceilometer/Aeronet extinction profiles at 360 nm (left) and 477 (right) with respect to scaled (top) and convoluted (bottom) Ceilometer profiles for all available FRM$_4$DOAS stations. Boxes and whiskers show the (25 - 75)th and (5 – 95)th percentile, respectively, in each retrieval layer. Median and mean of the data are shown as orange vertical bars and red open circles, respectively. Only profiles where both MMF and MAPA flags are valid are considered.

The distribution of the bias between extinction profiles from FRM$_4$DOAS and co-located Ceilometer measurements in each altitude level is shown in Figure 11 as box-whisker plots, and additionally in Figure 12 with the x-axis in symlog scale. Note that the data shown here is only from a subset of the AOD comparison in Section 4 since only data points are considered where not only both MMF and MAPA indicate validity (as for the AOD), but where also coincident Ceilometer and sun photometer measurements are available.

In general, extinction profiles are in good agreement both with scaled and convoluted Ceilometer profiles, with a slightly better agreement with convoluted profiles than with scaled profiles at higher altitudes. Both algorithms show a positive bias at the surface for the UV retrieval of about 0.02 km^{-1} and 0.06 km^{-1} for MMF and MAPA, respectively, which is compensated by a negative bias at higher altitudes by MMF and MAPA SF0.8. In particular in the UV, the difference to the ceilometer extinction is generally higher for MAPA than for MMF. In the visible, MMF exhibits several positive outliers in the uppermost retrieval layers, indicating an instability of the retrieval algorithm at these altitudes. The bias between MMF and Ceilometer in the lowermost 0-200 m retrieval layer is larger than for the layers above. This is most likely due to the fact that the Ceilometer has limited sensitivity to the lowermost 50-100 m.

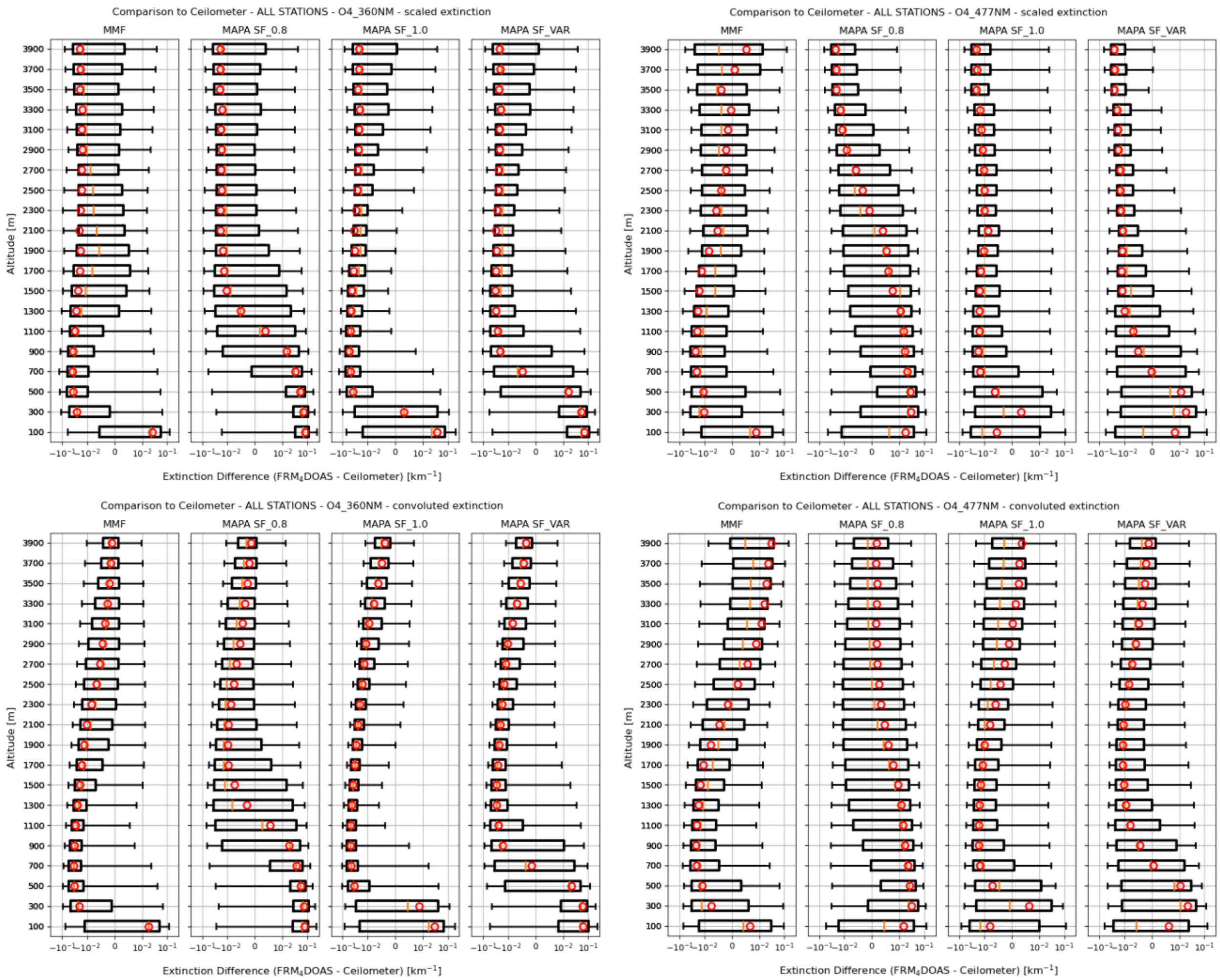

Figure 12: Same as Figure 8, but x-Axis in symlog scale, with a linear scale for -0.01 km^{-1} < x < 0.01 km^{-1}, and a logarithmic scale for |x| > 0.01 km^{-1}. Note that, in contrast to Figure 8, the apparent size of the boxes and whiskers does not correspond to the number of datapoints in each of the percentile intervals.

5.3 Extinction profile errors

The extinction profile errors for each layer reported by the different FRM_4DOAS algorithms is shown in Figure 13. The errors reported for most of the MMF profiles is below 0.1 km^{-1}, which is consistent with the bias between MMF and Ceilometer shown in Figure 12. The reduction of the MMF error with altitude reflects the fact that the sensitivity of the measurements decreases with altitude. Thus, the retrieval error approaches the a priori error at the top of the retrieval domain. Except for MAPA_VAR, the MAPA retrieval errors are also usually below 0.1 km^{-1}, but cover a broad range of error values with a surprisingly large number (~5%) of error values below 0.01 km^{-1}, and some even below 0.001 km^{-1}, which probably represents an underestimation of the true error. There is little variation of the MAPA error with altitude, with a tendency to lower errors at higher altitudes. Given that the MAPA algorithm does not rely on a priori information, this is a surprising finding since one would expect an increase of the error with altitude due to the decreasing sensitivity to aerosols.

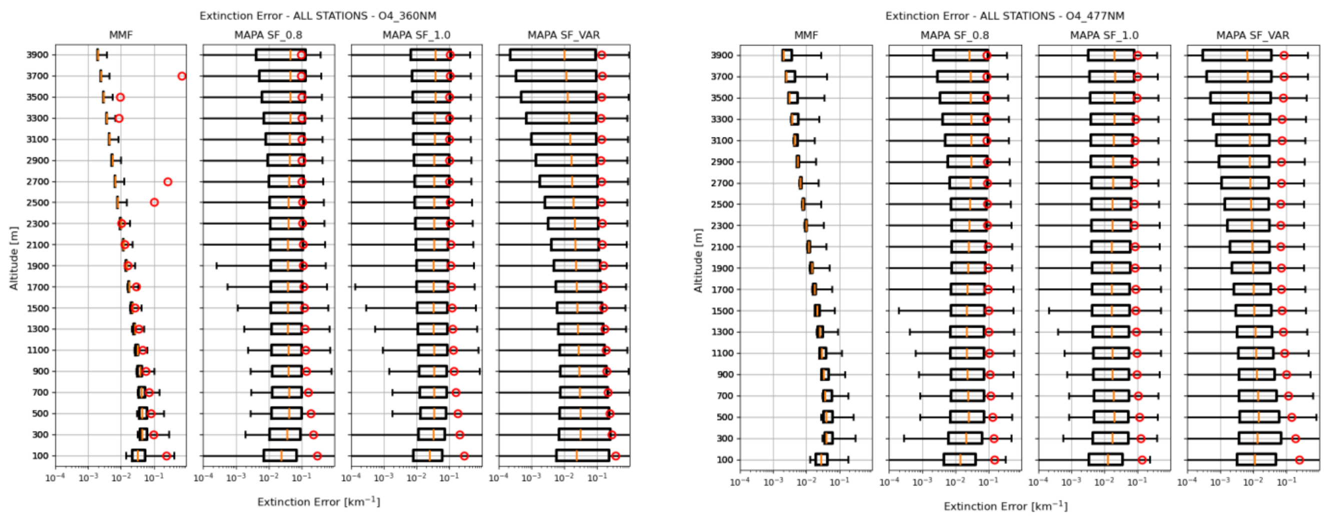

Figure 13: Reported extinction profile errors as a function of altitude for the different FRM_4DOAS Data products. Note the logarithmic x-axis scale.

6 Additional Tasks

6.1 Determination of the optimal viewing geometry

The choice of the elevation angle sequence for which MAX-DOAS measurements are performed strongly affects the information content of the aerosol and trace gas retrieval. It is therefore useful to investigate the minimum number of elevation angles and the suitable elevation angle values in order to get optimal information on the atmospheric state in as little measurement time as possible. Owing to the impact of aerosol scattering on the light path, the optimal elevation angle sequence will depend on the aerosol distribution in the atmosphere. This aspect has been investigated by varying the elevation angles for a sequence with a given number of viewing directions in order to maximise the DOFS of the retrieval using a Levenberg-Marquard algorithm. The optimisation has been done using the RAPSODI profile retrieval algorithm (Tirpitz et al., 2022) with a variety of different profile shapes, of which only two are discussed here: (1) a box profile with constant aerosol extinction from 0 to 250 m and zero above, and (2) a Gaussian shaped elevated aerosol profile centred at 1 km altitude with a thickness of σ = 500 m. The optimisation was done using 20 different AOD values and sequences of 1 to 5 off-axis angles (in addition to the zenith reference measurements).

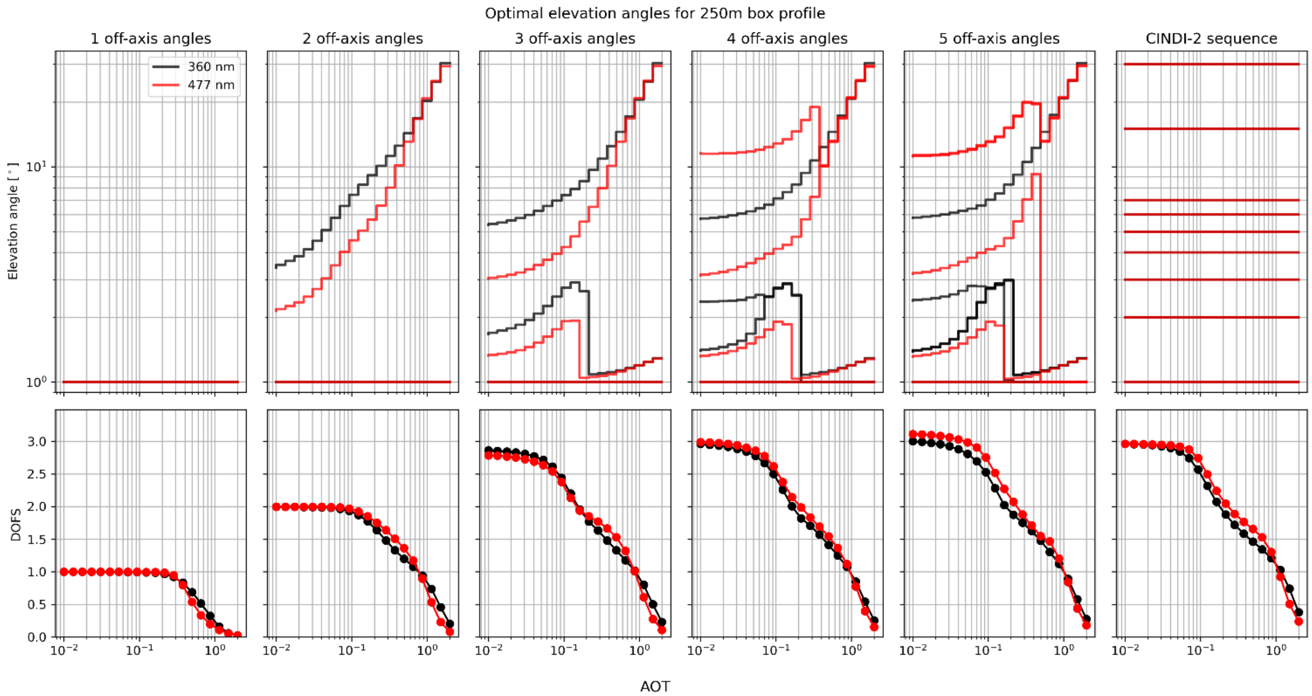

Figure 14: Optimal elevation angles (top) and information content (bottom) for sequences of 1-5 elevation angles (columns) as well as for the prescribed elevation angle sequence during the CINDI-2 and CINDI-3 campaign (rightmost column) as a function of AOD for a box-shaped aerosol profile of 250 m thickness.

Further settings for the radiative transfer simulations are as follows:

- RAA of 90° (the dependency of the RAA on the information content is quite weak)
- Logarithmic height grid with 25 layers between 0 and 7.5 km
- A priori aerosol profile error of 50% with a correlation length of 1 km
- Henyey-Greenstein aerosol phase function with an asymmetry parameter of 0.69
- Aerosol single scattering albedo of 0.91
- Surface albedo of 0.04

The resulting optimal elevation angles for the 250 m box aerosol profile for different numbers of elevation angles n between 1 and 5 are shown in Figure 14. Obviously, the lowest elevation angle should always be as close to the horizon as possible (in our simulations it is restricted to values >= 1°). The optimal elevation angles of the other viewing directions strongly depend on the aerosol load. The pointing should in general be higher up the higher the aerosol extinction. At low AOD, the DOFS is equal to the number of elevation angles. For $n > 1$, the DOFS remains at a constant value of 1 up to an AOD of about 0.1, and then decreases with increasing aerosol load. Almost no information on the aerosol distribution is available if the AOD exceeds 10 for any number of elevation angles in the sequence. The study shows that the 3 elevation angles are sufficient to fully exploit the information content of MAX-DOAS measurements, as the information content does not increase if more elevation angles are added. This requires, however, that the optimal viewing angle sequence is always chosen and thus that a viewing angle optimisation would be done in real time during the measurements. This is probably not a suitable approach for operational MAX-DOAS measurements. Instead, a larger number of elevation angles can be chosen which yields high content under many different atmospheric scenarios. Using the elevation angle sequence of the CINDI-2 and CINDI-3 campaign (1, 2, 3, 4, 6, 8, 15, 30, 90°) yields DOFS values similar to the optimised sequences for $n \geq 3$, and thus fully exploits the information content on aerosols, but with the disadvantage of a relatively long sampling time of 10 minutes per sequence.

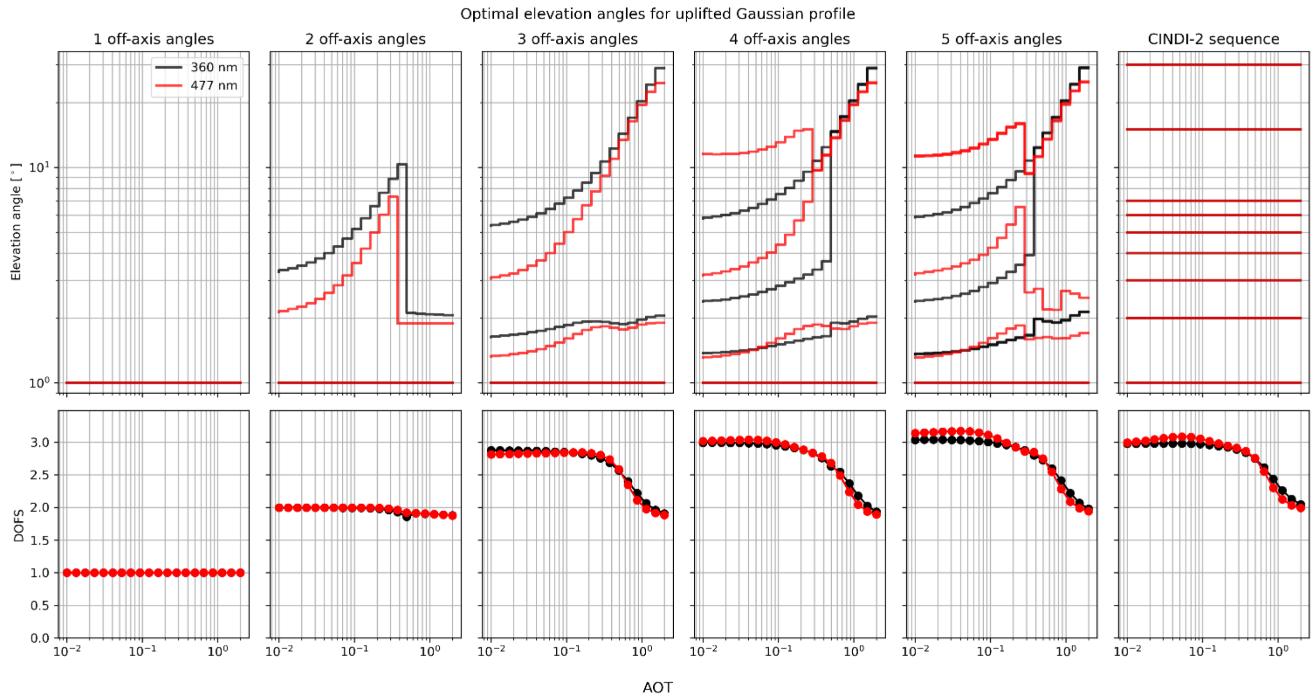

Figure 15: Same as Figure 14, but for an uplifted Gaussian profile centred at 1 km altitude.

The optimal viewing directions for for an uplifted Gaussian profile centred at 1 km altitude are shown in Figure 15. In this case, the information content depends much less on the aerosol content and a DOFS of 2 is achievable for n >=2 even at an AOD of 10 (which would correspond to a cloud at 1 km altitude).

6.2 Choice of the retrieval vertical grid

The currently implemented vertical grid with layers of 200 m between surface and 4 km altitude yields a relatively coarse representation of the aerosol extinction profile. The averaging kernels show that the vertical resolution near the surface is rather 50 m during clear sky conditions. Furthermore, the vertical resolution decreases with altitude, and a vertical grid with a layer thickness that increases with altitude, such as a logarithmic height grid, would be favourable because the information content would be distributed more evenly over the individual layers. It would furthermore allow to include the free troposphere with a limited number of layers, which is currently not part of the MMF state vector, but can have a significant impact on the MAX-DOAS measurements, e.g. by high-altitude cirrus clouds or uplifted aerosol layers.

The impact of the choice of the altitude grid, and also of the O_4 scaling factor, on the retrieval has been investigated using the RAPSODI retrieval algorithm. dSCDs measured at 477 nm at the Uccle station taken from the FRM$_4$DOAS L1 files for several days with different aerosol loads (low and moderate aerosols, fog and high-altitude clouds) serve as input for the retrieval. Retrievals were performed using linear grids with (1) 100 m and (2) 200 m layer thickness from 0 – 2 km and 0 – 4 km altitude, respectively, as well as (3) a logarithmic grid with 50 m layer thickness at the surface and 25 layers up to 9 km altitude. The resulting profiles were compared to the FRM$_4$DOAS operational products. Furthermore, the O_4 dSCDs modelled for the retrieved profiles were compared to the measured dSCDs. RAPSODI retrievals were performed using an O_4 scaling factor of 0.8 (standard) and 1.0. Here we restrict the discussion to a day with moderate aerosol load.

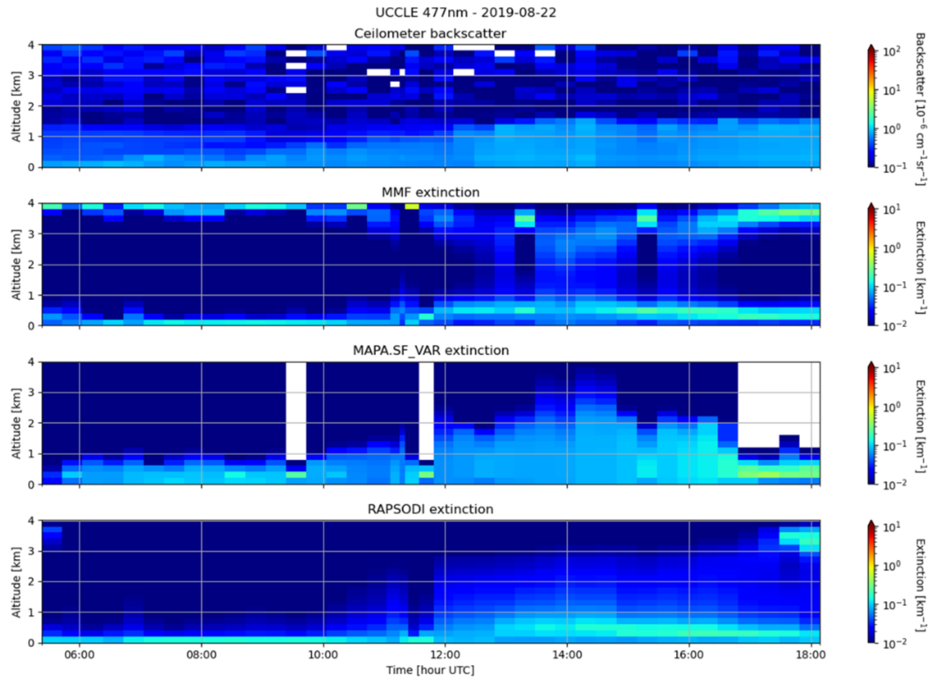

Figure 16: Aerosol extinction profiles for Uccle during moderate aerosol conditions. From top to bottom: (1) Ceilometer backscatter profile; (2) MMF extinction profile; (3) MAPA SF_VAR extinction profile (4) RAPSODI extinction profile with a scaling factor of 0.8. All retrievals were performed on the FRM$_4$DOAS standard altitude grid (200 m layers from 0-4 km).

Figure 16 shows a comparison of Ceilometer, MMF, MAPA SF_VAR and RAPSODI on the 200 m standard grid for Uccle during moderate aerosol conditions. All algorithms exhibit a similar vertical structure with enhanced aerosols near the surface, with a shallow layer during the morning whose vertical extent increases in the afternoon. The vertical profiles from RAPSODI, and in particular from MMF, appear less blurred than those of MAPA. However, MMF shows enhanced extinction values in the uppermost retrieval layers, which seem to be an artefact that is not present in the Ceilometer profiles.

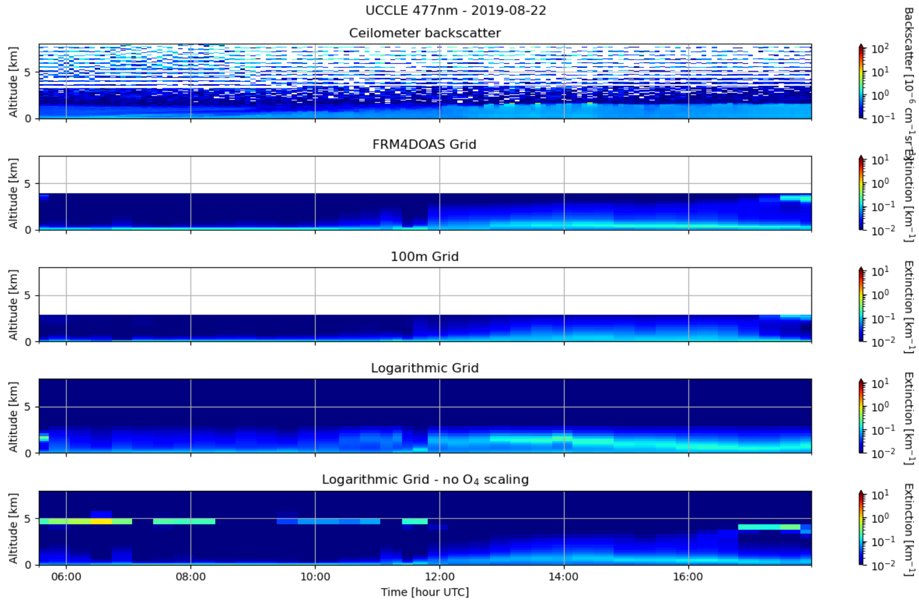

Figure 17: RAPSODI profiles using different altitude grids for the same day as in Figure 16. From top to bottom: (1) Ceilometer backscatter profiles; (2) FRM_4DOAS standard grid with 200 m resolution; (3) 100 m grid; (4) Logarithmic grid; (5) Logarithmic grid with a scaling factor of 1.0 instead of 0.8. Note the different y-axis scale (0 – 9 km) compared to Figure 16 (0 – 4 km).

Figure 17 shows extinction profiles retrieved by RAPSODI using different altitude grids. The vertical structure of aerosol profiles can be retrieved by any of the chosen grids when applying an O_4 scaling factor of 0.8m whereas unreasonably high extinction values are retrieved at the altitude layer right below 5 km if no O_4 scaling is applied.

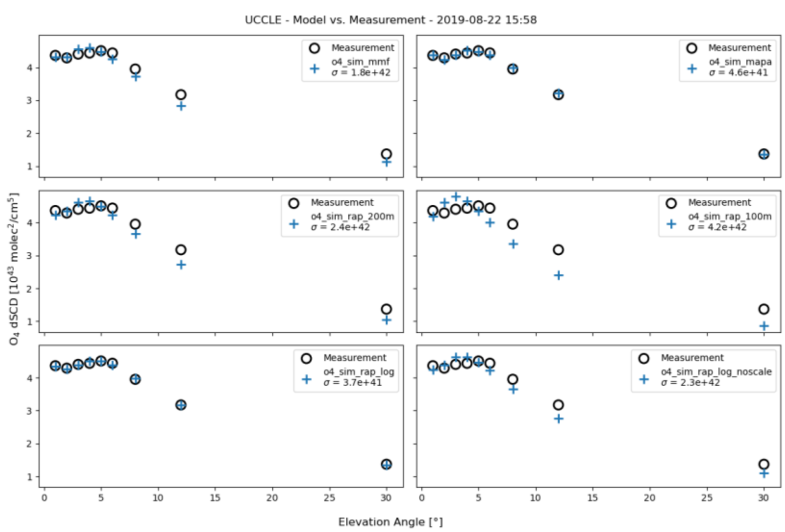

Figure 18: Comparison between measured and simulated O_4 dSCDs for a single vertical profile in the afternoon of 22. August 2019 at Uccle. The different panels show: o4_mmf: simulated dSCDs for the MMF operational product; o4_sim_mapa: simulated dSCDs for the MAPA SF_VAR operational product; o4_sim_rap_200m: simulated dSCDs from RAPSODI for the 200 m grid; o4_sim_rap_100m: simulated dSCDs from RAPSODI for the 100 m grid; o4_sim_rap_log: simulated dSCDs from RAPSODI for the logarithmic grid; o4_sim_rap_log_noscale: simulated dSCDs from RAPSODI for the logarithmic grid, but without O_4 scaling.

The comparison between measured and simulated O_4 dSCDs for the FRM_4DOAS operational products as well as the RAPSODI retrievals on different grids and with and without scaling factor is shown in Figure 18. Reasonable convergence between model and measurement can only be achieved if both the free troposphere is included in the retrieval and if an O_4 scaling factor is applied, which is the case for MAPA SF_VAR (top left panel) and RAPSODI o4_sim_rap_log (lower left panel). Insufficient convergence is achieved in all other cases when either the free troposphere is not included or no scaling of the O_4 cross section is applied.

In summary, it can be stated that the currently implemented 200 m altitude grid is unreasonably coarse. It does not reflect the high sensitivity of MAX-DOAS measurements near the surface appropriately, where structures with a vertical extent of about 50 m could be resolved using a finer vertical grid. On the other hand, aerosols and clouds above the currently implemented grid (4 km) have a significant impact on the O_4 dSCDs. Together with the lack of an O_4 scaling factor, this causes artefacts in the uppermost layers of the MMF profiles. Logarithmic height grids may solve these problems because they can cover the entire troposphere with a reasonably small number of layers and they lead to a more evenly distributed information content over each of the layers.

6.3 Impact of the surface albedo on the aerosol retrieval

Currently, the surface albedo in the FRM$_4$DOAS operational retrieval is set to a fixed value for each station. This can be problematic if a wrong albedo value not representative for the particular site is chosen, or even more if the surface albedo changes with time, for example due to the presence of a snow cover during winter. The impact of the surface albedo on the MAX-DOAS profile retrieval has been investigated based on measurements of the IUP-HD PMAX-DOAS instrument during the CINDI-3 campaign in Cabauw, the Netherlands, using data from 5. June 2024. Two profile retrieval runs were performed: (1) a retrieval run using a fixed surface albedo of 0.06, and (2) a retrieval run in which the surface albedo was retrieved with quite loose a priori constraints (0.06 +/- 0.1). Note that, as during the entire campaign, the weather conditions were not favourable on this day when varying cloud cover was present.

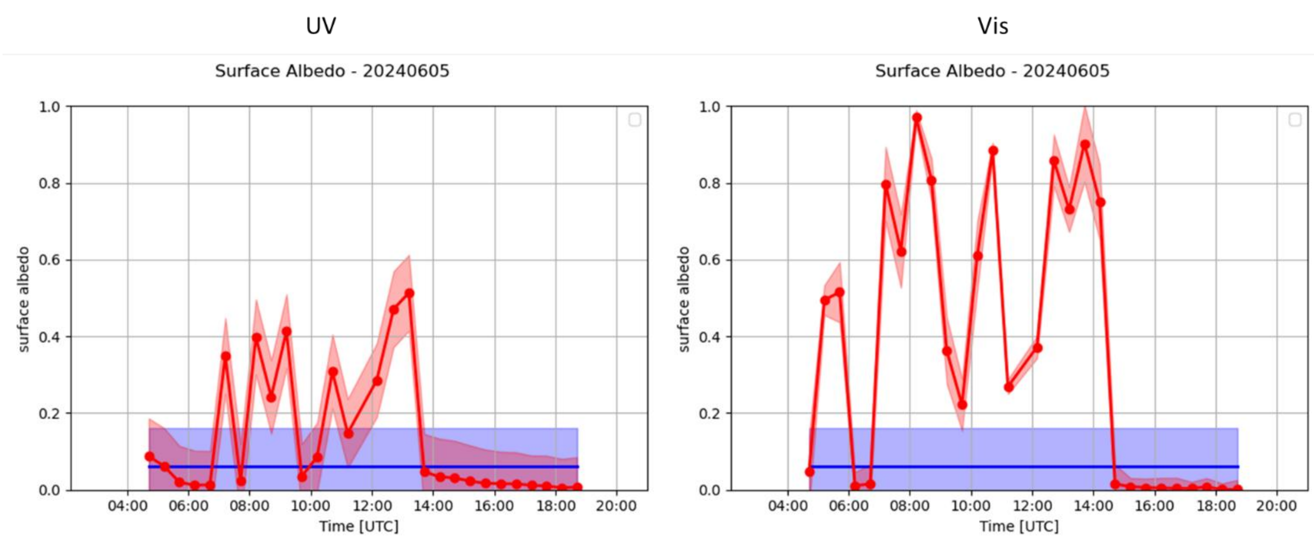

Figure 19: A priori (blue) and a posteriori (red) albedo values for the profile retrieval on 5. June 2024 in Cabauw, The Netherlands, in the UV (left) and visible (right). The solid lines show the albedo values, and the shaded areas the a priori and a posteriori errors, respectively.

The a priori and retrieved albedo values for this day shown in Figure 19 indicate that the surface albedo cannot be retrieved reliably under cloudy conditions, during which the values strongly fluctuate and yield unreasonably high values. The retrieved albedo shows more realistic values below 0.1 after about 2 pm, when less clouds are present. The vertical profiles of aerosols and trace gases using both fixed and variable albedo values shown in Figure 15 and 16 indicate that the impact of surface albedo on the retrieved profiles is small. The same applies to the NO_2 surface VMR shown in Figure 22. It can therefore be concluded that there is only a small impact of a wrongly chosen albedo value on the retrieved profiles.

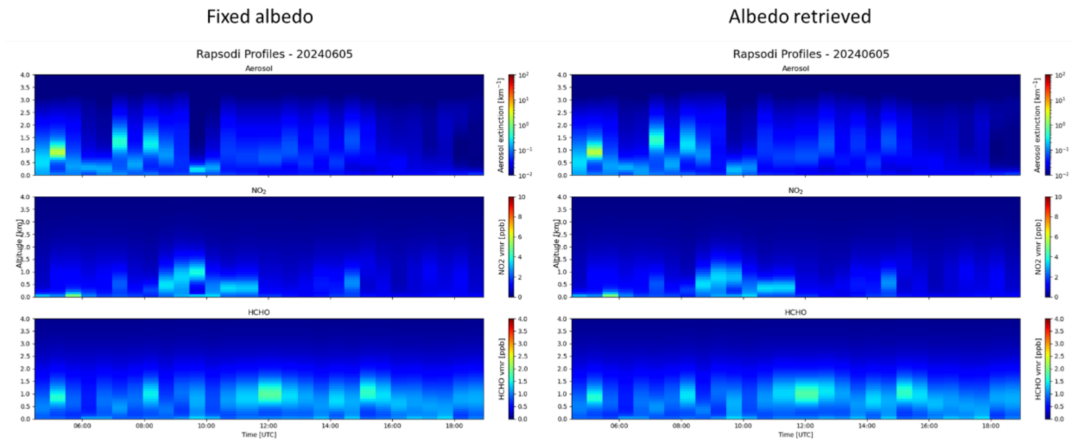

Figure 20: Retrieved vertical profiles iof aerosol extinction (top), NO_2 (centre) and formaldehyde (bottom) in the UV spectral region on 5. June 2024 using fixed (left) and variable (right) surface albedo.

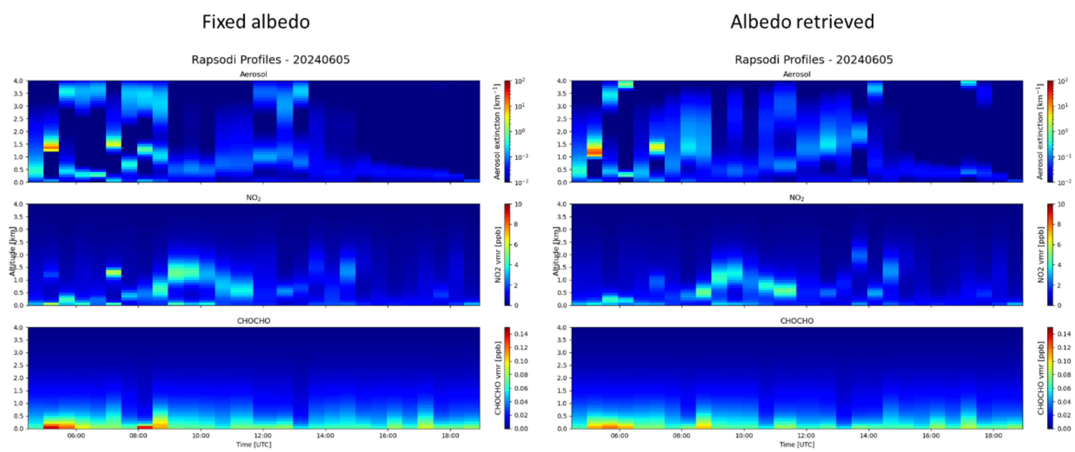

Figure 21: Same as Figure 20, but for aerosols, NO_2 and glyoxal in the visible wavelength range.

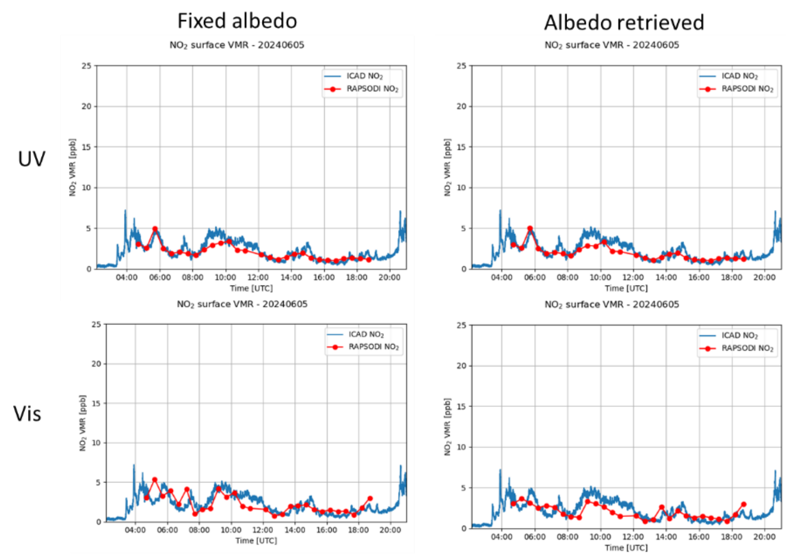

Figure 22: Comparison of retrieved NO2 surface VMR with in situ ICAD measurements on 5. June 2024 in the UV (top) and visible (bottom) using a fixed (left) and variable (right) albedo value.

7 Summary and Recommendations for improved FRM$_4$DOAS aerosol retrieval schemes

The findings of this validation study yield a number of issues that should be addressed for an improvement of the FRM$_4$DOAS aerosol retrieval scheme. These can be subdivided into tasks of high and medium importance, as well as optional improvements of the FRM$_4$DOAS processor:

High importance

- The MMF flagging scheme is too strict, with only a very small amount of MMF profiles (< 0.1%) are flagged as valid. The MMF QA flag therefore needs to be revised in order to make a reasonable number of valid profiles available for the end user.
- MMF systematically underestimates the AOD by about factor of two. The reasons for this discrepancy, which potentially include the choice of the aerosol a priori profile, and/or a lack of scaling of the O_4 cross sections, need to be identified in order to resolve this problem.
- The AOD of the MAPA aerosol data product is not in agreement with the integrated extinction profiles. This is to be expected since the MAPA parametrised approach also includes aerosols above 4 km. The inconsistency between profiles and AOD from MAPA output in FRM4DOAS is resolved by a revised configuration file that needs to be included in the next update of the FRM4DOAS processor.
- The comparison of FRM$_4$DOAS aerosol extinction profiles with ceilometer measurements reveals that MAPA frequently shows positive outliers for the variable scaling factor scheme. The reasons for this behaviour is probably related to the additional degree of freedom and should be investigated and, if possible, resolved.

Medium importance

- The height grid of the FRM_4DOAS profile retrieval is relatively coarse with a layer thickness of 200 m. A finer height grid (e.g., 100 m layer thickness) would enable to resolve gradients in the aerosol (and trace gas) profiles, in particular near the surface, where shallow layers frequently occur, in particular during the morning hours in the presence of strong inversions. Alternatively, a logarithmic height grid where the layer thickness increases with altitude can provide high spatial resolution near the ground using a relatively small number of retrieval layers. A logarithmic height grid would also enable to retrieve some (limited) information on aerosols in the free troposphere.
- The question whether a scaling factor should be applied to the O_4 dSCDs is an ongoing discussion in the DOAS community. It is not possible to draw any substantial conclusions on this issue from this validation study. The correlation of the MAPA AOD with sun photometer measurements is worst if no scaling factor is applied. In the UV, the correlation is slightly better with a fixed scaling factor of 0.8 than with a variable scaling factor

Optional tasks

- It has been shown in the past that measurements from elevated locations, such as hilltops, can gain additional information on trace gases and aerosols below the observer when pointing the MAX-DOAS telescope downwards [Frieß et al, 2023]. It would therefore be useful if the FRM_4DOAS processor would accept measurements at negative elevation angles.
- The retrieval of aerosol microphysical and/or optical properties from MAX-DOAS azimuth or almucantar scans would be an innovative extension of the FRM_4DOAS processor. This is, however, outside the scope of this project.

8 References

Beirle, S., Dörner, S., Donner, S., Remmers, J., Wang, Y., and Wagner, T.: The Mainz profile algorithm (MAPA), Atmos. Meas. Tech., 12, 1785–1806, https://doi.org/10.5194/amt-12-1785-2019, 2019.

Friedrich, M. M., Rivera, C., Stremme, W., Ojeda, Z., Arellano, J., Bezanilla, A., García-Reynoso, J. A., and Grutter, M.: NO_2 vertical profiles and column densities from MAX-DOAS measurements in Mexico City, Atmos. Meas. Tech., 12, 2545–2565, https://doi.org/10.5194/amt-12-2545-2019, 2019.

Frieß, U., Kreher, K., Querel, R., Schmithüsen, H., Smale, D., Weller, R., and Platt, U.: Source mechanisms and transport patterns of tropospheric bromine monoxide: findings from long-term multi-axis differential optical absorption spectroscopy measurements at two Antarctic stations, Atmospheric Chemistry and Physics, 23, 3207–3232, https://doi.org/10.5194/acp-23-3207-2023, 2023.

Rodgers, C. D. and Connor, B. J.: Intercomparison of remote sounding instruments, J. Geophys. Res, 108, 4116–4229, https://doi.org/10.1029/2002JD002299, 2003.

Tirpitz, J.-L., Frieß, U., Hendrick, F., Alberti, C., Allaart, M., Apituley, A., Bais, A., Beirle, S., Berkhout, S., Bognar, K., Bösch, T., Bruchkouski, I., Cede, A., Chan, K. L., den Hoed, M., Donner, S., Drosoglou, T., Fayt, C., Friedrich, M. M., Frumau, A., Gast, L., Gielen, C., Gomez-Martín, L., Hao, N., Hensen, A., Henzing, B., Hermans, C., Jin, J., Kreher, K., Kuhn, J., Lampel, J., Li, A., Liu, C., Liu, H., Ma, J., Merlaud, A., Peters, E., Pinardi, G., Piters, A., Platt, U., Puentedura, O., Richter, A., Schmitt, S., Spinei, E., Stein Zweers, D., Strong, K., Swart, D., Tack, F., Tiefengraber, M., van der Hoff, R., van Roozendael, M., Vlemmix, T., Vonk, J., Wagner, T., Wang, Y., Wang, Z., Wenig, M., Wiegner, M., Wittrock, F., Xie, P., Xing, C., Xu, J., Yela, M., Zhang, C., and Zhao, X.: Intercomparison of MAX-DOAS vertical profile retrieval algorithms: studies on field data from the CINDI-2 campaign, Atmospheric Measurement Techniques, 14, 1–35, https://doi.org/10.5194/amt-14-1-2021, 2021.

Tirpitz, J.-L., Frieß, U., Spurr, R., and Platt, U.: Enhancing MAX-DOAS atmospheric state retrievals by multispectral polarimetry – studies using synthetic data, Atmospheric Measurement Techniques, 15, 2077–2098, https://doi.org/10.5194/amt-15-2077-2022, 2022.

9 Appendix

9.1 Correlation of MMF with MAPA AOD for each station

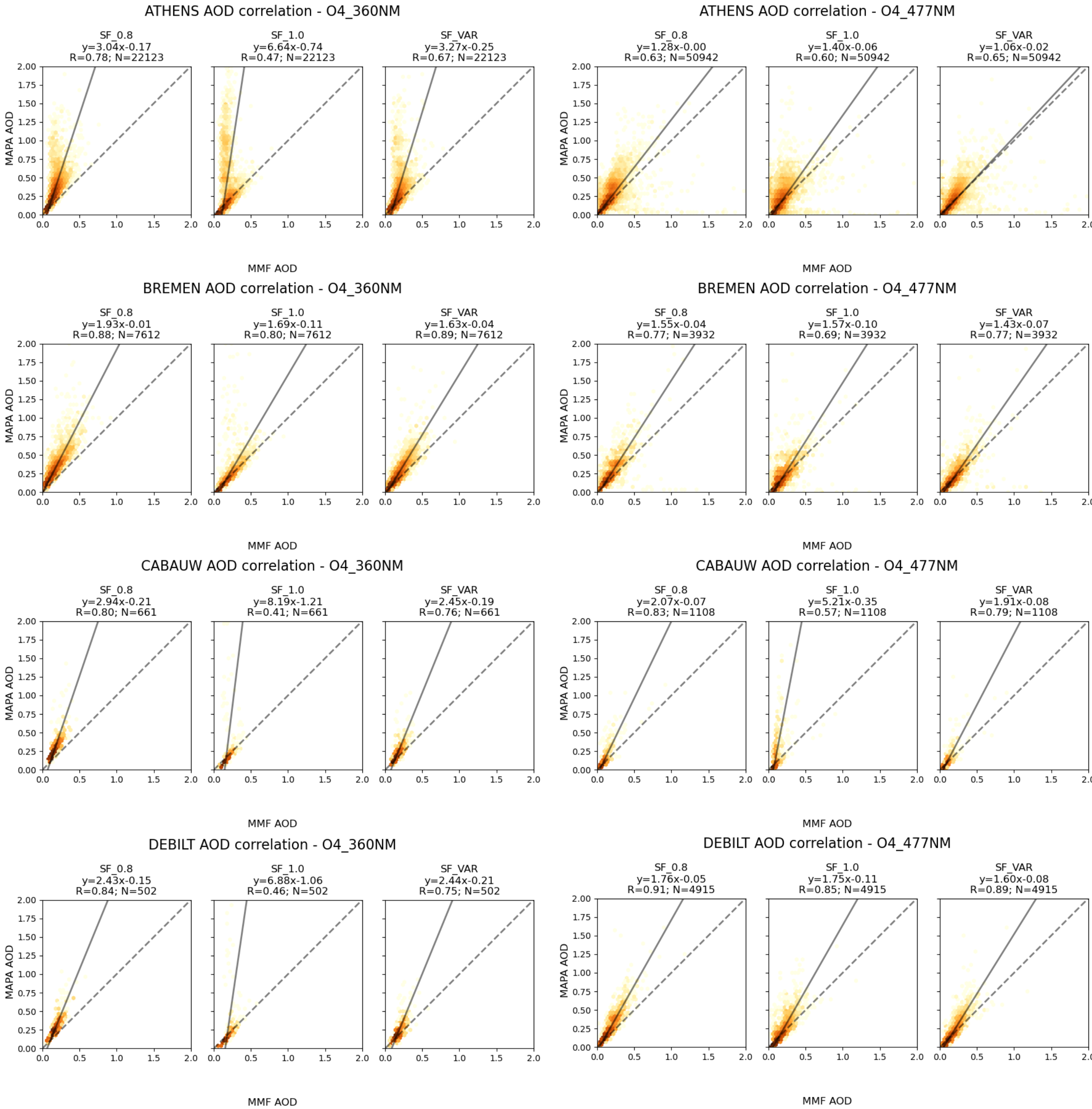

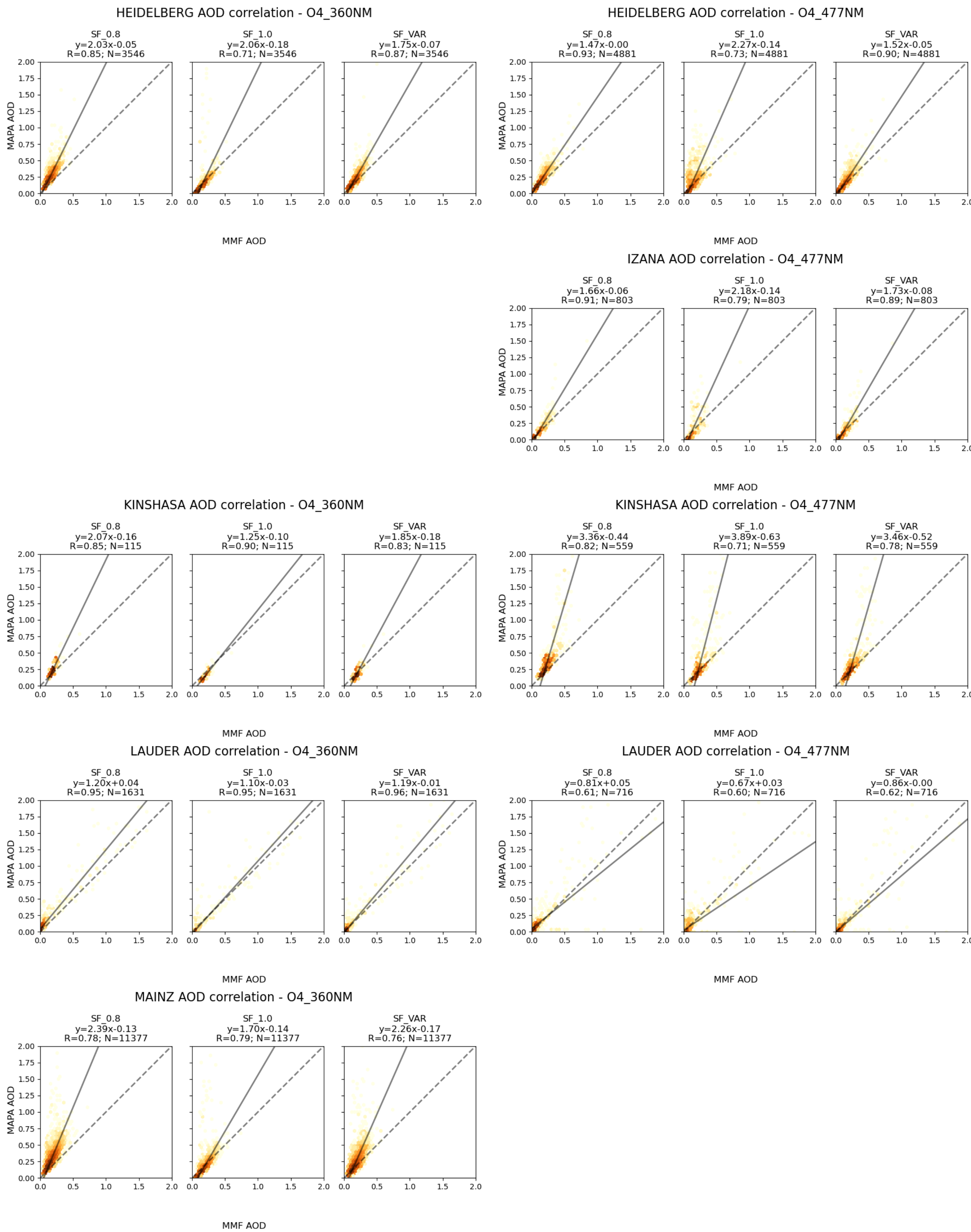
HEIDELBERG AOD correlation - O4_360NM
SF_0.8
y=2.03x-0.05
R=0.85; N=3546
SF_1.0
y=2.06x-0.18
R=0.71; N=3546
SF_VAR
y=1.75x-0.07
R=0.87; N=3546
MAPA AOD
MMF AOD
HEIDELBERG AOD correlation - O4_477NM
SF_0.8
y=1.47x-0.00
R=0.93; N=4881
SF_1.0
y=2.27x-0.14
R=0.73; N=4881
SF_VAR
y=1.52x-0.05
R=0.90; N=4881
MAPA AOD
MMF AOD
IZANA AOD correlation - O4_477NM
SF_0.8
y=1.66x-0.06
R=0.91; N=803
SF_1.0
y=2.18x-0.14
R=0.79; N=803
SF_VAR
y=1.73x-0.08
R=0.89; N=803
MAPA AOD
MMF AOD
KINSHASA AOD correlation - O4_360NM
SF_0.8
y=2.07x-0.16
R=0.85; N=115
SF_1.0
y=1.25x-0.10
R=0.90; N=115
SF_VAR
y=1.85x-0.18
R=0.83; N=115
MAPA AOD
MMF AOD
KINSHASA AOD correlation - O4_477NM
SF_0.8
y=3.36x-0.44
R=0.82; N=559
SF_1.0
y=3.89x-0.63
R=0.71; N=559
SF_VAR
y=3.46x-0.52
R=0.78; N=559
MAPA AOD
MMF AOD
LAUDER AOD correlation - O4_360NM
SF_0.8
y=1.20x+0.04
R=0.95; N=1631
SF_1.0
y=1.10x-0.03
R=0.95; N=1631
SF_VAR
y=1.19x-0.01
R=0.96; N=1631
MAPA AOD
MMF AOD
LAUDER AOD correlation - O4_477NM
SF_0.8
y=0.81x+0.05
R=0.61; N=716
SF_1.0
y=0.67x+0.03
R=0.60; N=716
SF_VAR
y=0.86x-0.00
R=0.62; N=716
MAPA AOD
MMF AOD
MAINZ AOD correlation - O4_360NM
SF_0.8
y=2.39x-0.13
R=0.78; N=11377
SF_1.0
y=1.70x-0.14
R=0.79; N=11377
SF_VAR
y=2.26x-0.17
R=0.76; N=11377
MAPA AOD
MMF AOD

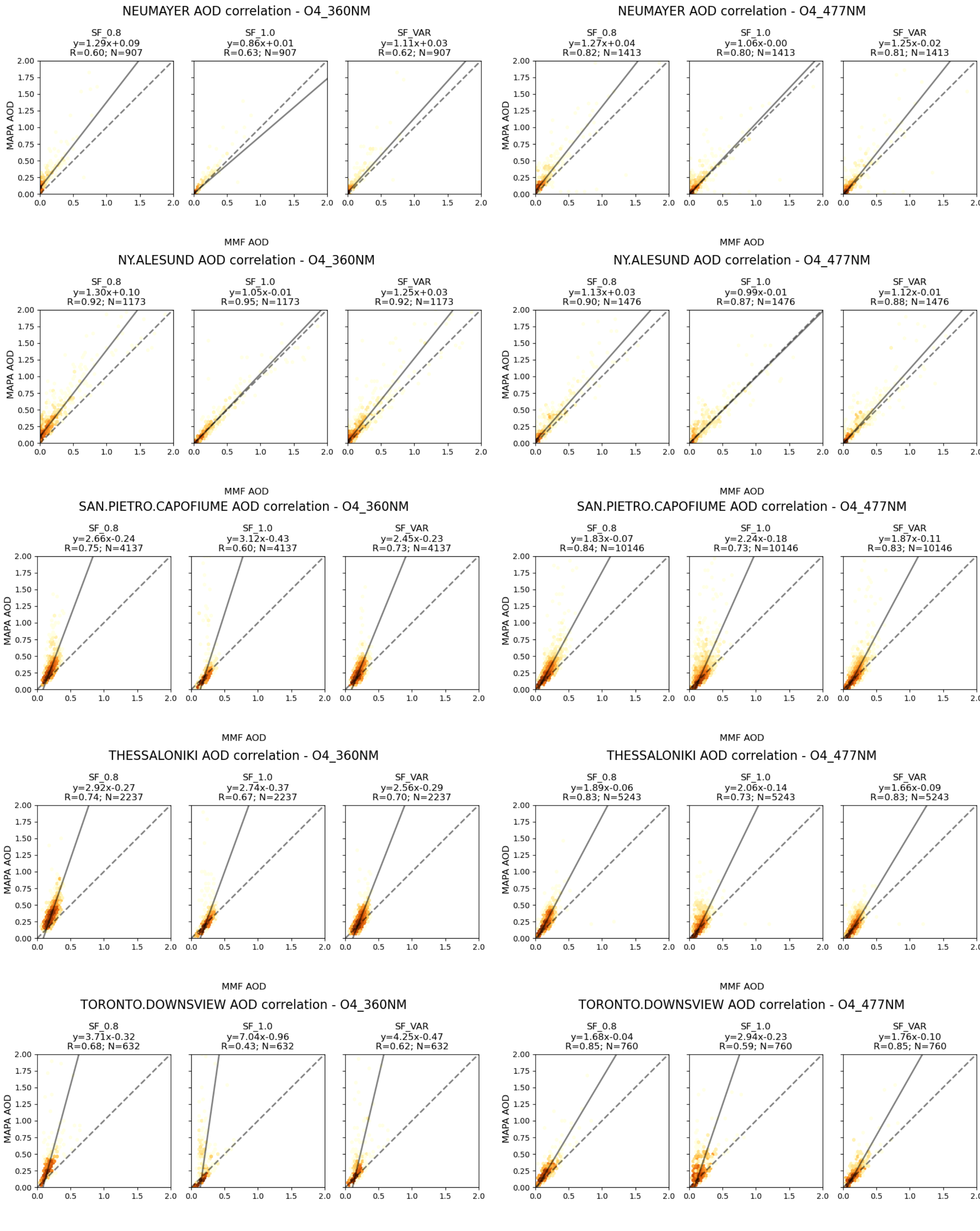
NEUMAYER AOD correlation - O4_360NM
SF_0.8
y=1.29x+0.09
R=0.60; N=907
SF_1.0
y=0.86x+0.01
R=0.63; N=907
SF_VAR
y=1.11x+0.03
R=0.62; N=907
NEUMAYER AOD correlation - O4_477NM
SF_0.8
y=1.27x+0.04
R=0.82; N=1413
SF_1.0
y=1.06x-0.00
R=0.80; N=1413
SF_VAR
y=1.25x-0.02
R=0.81; N=1413
NY.ALESUND AOD correlation - O4_360NM
SF_0.8
y=1.30x+0.10
R=0.92; N=1173
SF_1.0
y=1.05x-0.01
R=0.95; N=1173
SF_VAR
y=1.25x+0.03
R=0.92; N=1173
NY.ALESUND AOD correlation - O4_477NM
SF_0.8
y=1.13x+0.03
R=0.90; N=1476
SF_1.0
y=0.99x-0.01
R=0.87; N=1476
SF_VAR
y=1.12x-0.01
R=0.88; N=1476
SAN.PIETRO.CAPOFIUME AOD correlation - O4_360NM
SF_0.8
y=2.66x-0.24
R=0.75; N=4137
SF_1.0
y=3.12x-0.43
R=0.60; N=4137
SF_VAR
y=2.45x-0.23
R=0.73; N=4137
SAN.PIETRO.CAPOFIUME AOD correlation - O4_477NM
SF_0.8
y=1.83x-0.07
R=0.84; N=10146
SF_1.0
y=2.24x-0.18
R=0.73; N=10146
SF_VAR
y=1.87x-0.11
R=0.83; N=10146
THESSALONIKI AOD correlation - O4_360NM
SF_0.8
y=2.92x-0.27
R=0.74; N=2237
SF_1.0
y=2.74x-0.37
R=0.67; N=2237
SF_VAR
y=2.56x-0.29
R=0.70; N=2237
THESSALONIKI AOD correlation - O4_477NM
SF_0.8
y=1.89x-0.06
R=0.83; N=5243
SF_1.0
y=2.06x-0.14
R=0.73; N=5243
SF_VAR
y=1.66x-0.09
R=0.83; N=5243
TORONTO.DOWNSVIEW AOD correlation - O4_360NM
SF_0.8
y=3.71x-0.32
R=0.68; N=632
SF_1.0
y=7.04x-0.96
R=0.43; N=632
SF_VAR
y=4.25x-0.47
R=0.62; N=632
TORONTO.DOWNSVIEW AOD correlation - O4_477NM
SF_0.8
y=1.68x-0.04
R=0.85; N=760
SF_1.0
y=2.94x-0.23
R=0.59; N=760
SF_VAR
y=1.76x-0.10
R=0.85; N=760
MAPA AOD
MMF AOD

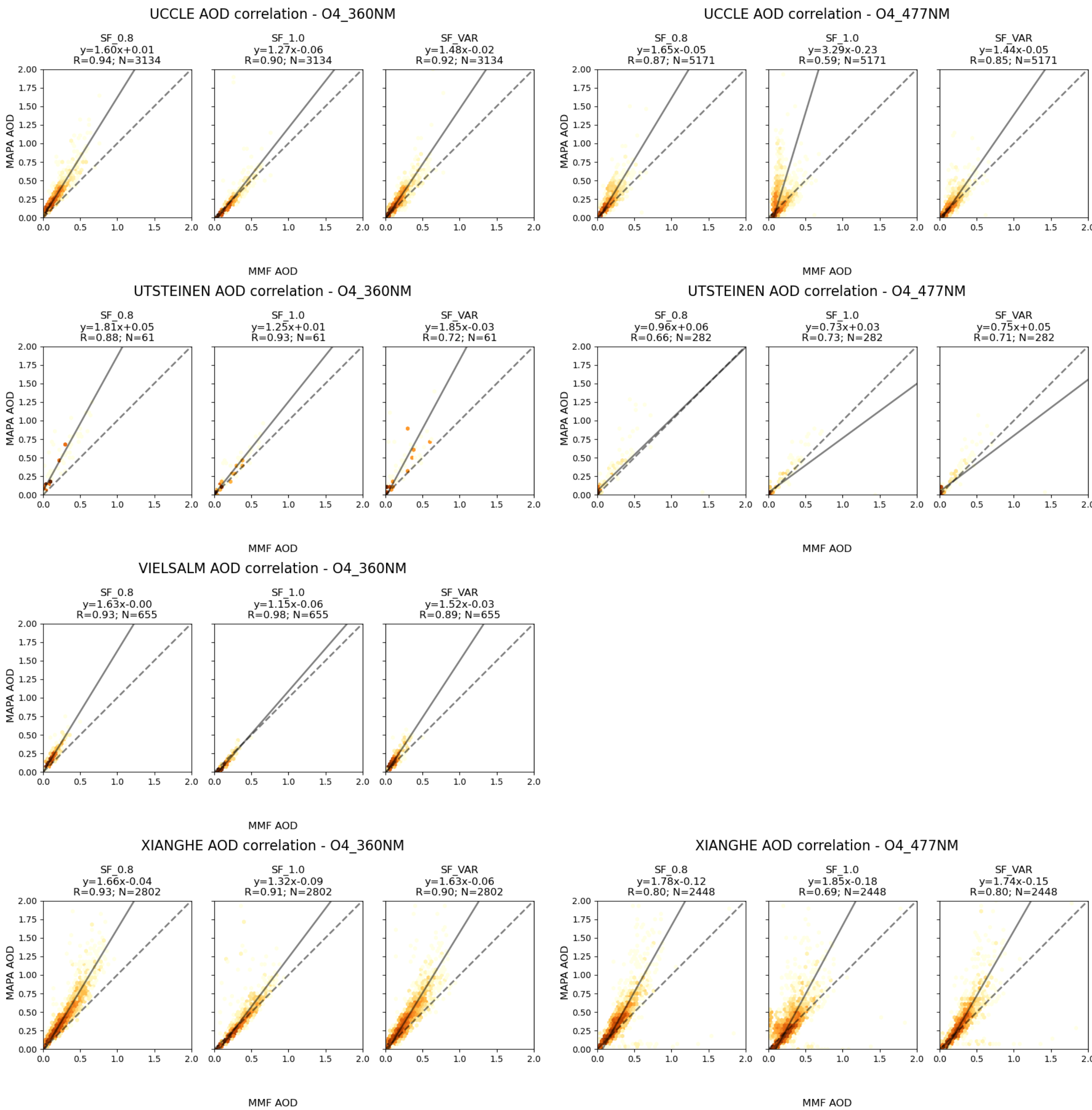
UCCLE AOD correlation - O4_360NM
SF_0.8
y=1.60x+0.01
R=0.94; N=3134
SF_1.0
y=1.27x-0.06
R=0.90; N=3134
SF_VAR
y=1.48x-0.02
R=0.92; N=3134
MAPA AOD
MMF AOD
UCCLE AOD correlation - O4_477NM
SF_0.8
y=1.65x-0.05
R=0.87; N=5171
SF_1.0
y=3.29x-0.23
R=0.59; N=5171
SF_VAR
y=1.44x-0.05
R=0.85; N=5171
MAPA AOD
MMF AOD
UTSTEINEN AOD correlation - O4_360NM
SF_0.8
y=1.81x+0.05
R=0.88; N=61
SF_1.0
y=1.25x+0.01
R=0.93; N=61
SF_VAR
y=1.85x-0.03
R=0.72; N=61
MAPA AOD
MMF AOD
UTSTEINEN AOD correlation - O4_477NM
SF_0.8
y=0.96x+0.06
R=0.66; N=282
SF_1.0
y=0.73x+0.03
R=0.73; N=282
SF_VAR
y=0.75x+0.05
R=0.71; N=282
MAPA AOD
MMF AOD
VIELSALM AOD correlation - O4_360NM
SF_0.8
y=1.63x-0.00
R=0.93; N=655
SF_1.0
y=1.15x-0.06
R=0.98; N=655
SF_VAR
y=1.52x-0.03
R=0.89; N=655
MAPA AOD
MMF AOD
XIANGHE AOD correlation - O4_360NM
SF_0.8
y=1.66x-0.04
R=0.93; N=2802
SF_1.0
y=1.32x-0.09
R=0.91; N=2802
SF_VAR
y=1.63x-0.06
R=0.90; N=2802
MAPA AOD
MMF AOD
XIANGHE AOD correlation - O4_477NM
SF_0.8
y=1.78x-0.12
R=0.80; N=2448
SF_1.0
y=1.85x-0.18
R=0.69; N=2448
SF_VAR
y=1.74x-0.15
R=0.80; N=2448
MAPA AOD
MMF AOD

9.2 Correlation of MMF and MAPA with Aeronet AOD for each station

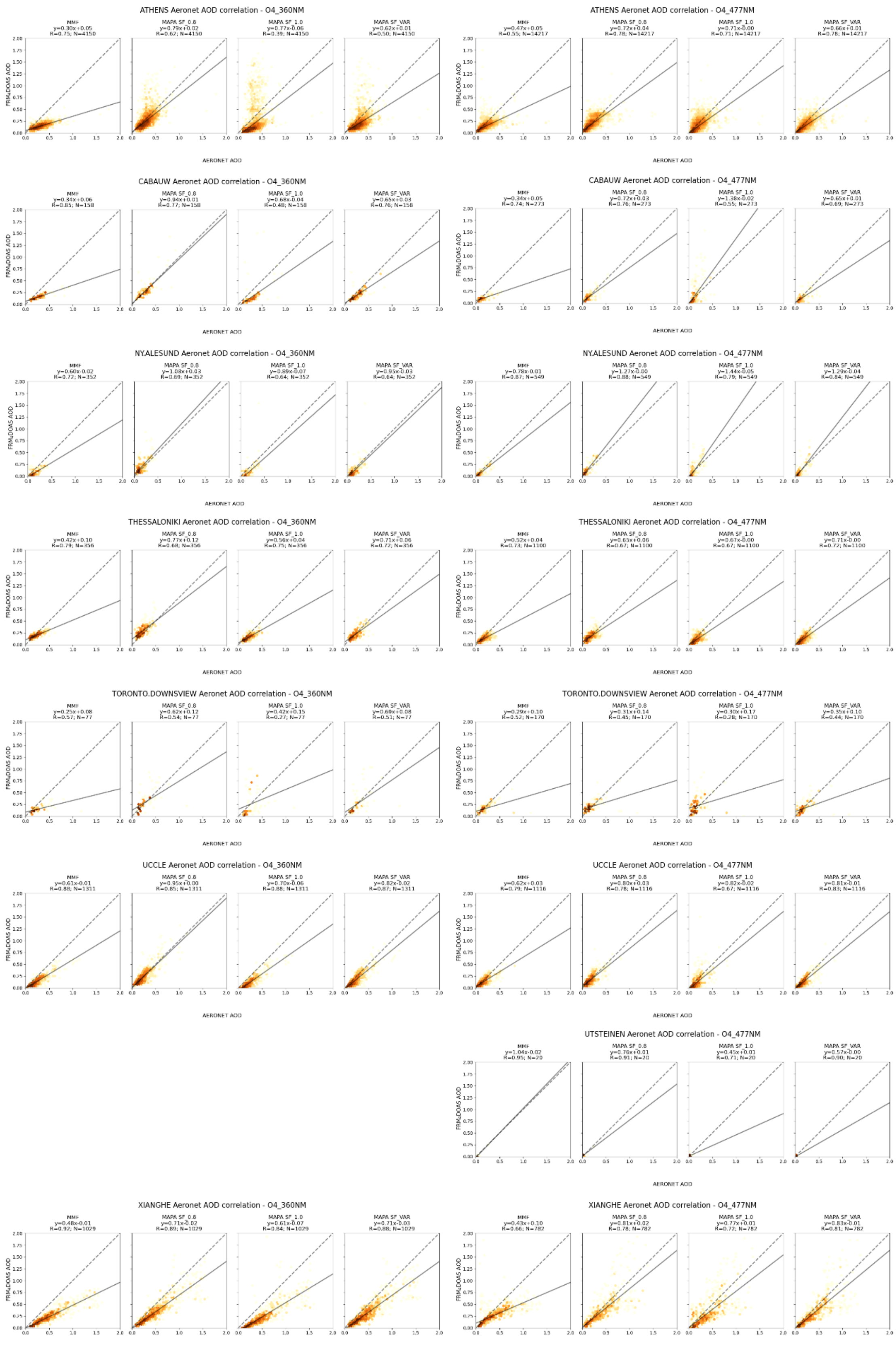

9.3 Bias between aerosol extinction profiles from FRM4DOAS and co-located Ceilometer instruments for each station